



Contents lists available at ScienceDirect

Saudi Pharmaceutical Journal

journal homepage: www.sciencedirect.com

Original article

Virtual screening and molecular dynamics simulation analysis of Forsythoside A as a plant-derived inhibitor of SARS-CoV-2 3CLpro

Shabana Bibi^{a,b,1,*}, Muhammad Saad Khan^{c,1}, Sherif A. El-Kafrawy^{d,e}, Thamir A. Alandijany^{d,e}, Mai M. El-Daly^{d,e}, Qudsia Yousafi^c, Dua Fatima^c, Arwa A. Faizo^{d,e}, Leena H. Bajrai^{d,f}, Esam I. Azhar^{d,e,*}

^a Department of Biosciences, Shifa-Tameer-e-Milat University, Islamabad, Pakistan

^b Yunnan Herbal Laboratory, College of Ecology and Environmental Sciences, Yunnan University, Kunming 650091, Yunnan, China

^c Department of Biosciences, COMSATS University Islamabad, Sahiwal, Pakistan

^d Special Infectious Agents Unit, King Fahd Medical Research Centre, King Abdulaziz University, Jeddah, Saudi Arabia

^e Department of Medical Laboratory Sciences, Faculty of Applied Medical Sciences, King Abdulaziz University, Jeddah, Saudi Arabia

^f Biochemistry Department, Faculty of Sciences, King Abdulaziz University, Jeddah, Saudi Arabia

ARTICLE INFO

Article history:

Received 7 February 2022

Accepted 20 May 2022

Available online 25 May 2022

Keywords:

COVID-19

Coronavirus

Molecular dynamic simulation

Molecular docking

ADMET

Natural compounds

3CLpro

SARS-CoV-2

ABSTRACT

Severe acute respiratory syndrome coronavirus-2 (SARS-CoV-2) is a more severe strain of coronavirus (CoV) that was first emerged in China in 2019. Available antiviral drugs could be repurposed and natural compounds with antiviral activity could be safer and cheaper source of medicine for SARS-CoV-2. 78 natural antiviral compounds database was identified from literature and virtual screening technique was applied to identify potential 3-chymotrypsin-like protease (3CLpro) inhibitors. Molecular docking studies were conducted to analyze the main protease (3CLpro) and inhibitors interactions with key residues of active site of target protein (PDB ID: 6LU7), active site constitute the part of active domain I and II of 3CLpro. 10 compounds with highest dock score were subjected to calculate ADMET parameters to figure out drug-likeness. Molecular dynamic (MD) simulation of the selected lead was performed by Amber simulation package to understand the conformational changes in docked complex. MD simulations analysis (RMSD, RMSF, Rg, BF, HBs, and SASA plots) of lead bounded with 3CLpro, hence revealed the important structural turns and twists during MD simulations from 0 to 100 ns. MM-PBSA/GBSA methods has also been applied for the estimation binding free energy (BFE) of the selected lead-complex. The present study has identified lead compound "Forsythoside A" an active extract of *Forsythia suspense* as SARS-CoV-2 3CLpro inhibitor that can block the viral replication and translation. Structural analysis of target protein and lead compound performed in this study could contribute to the development of potential drug against SARS-CoV-2 infection.

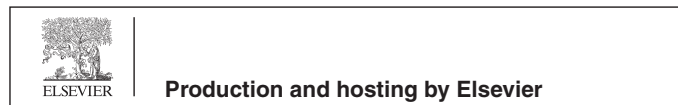
© 2022 Published by Elsevier B.V. on behalf of King Saud University. This is an open access article under the CC BY-NC-ND license (<http://creativecommons.org/licenses/by-nc-nd/4.0/>).

* Corresponding authors at: Department of Biosciences, Shifa-Tameer-e-Milat University, Islamabad, Pakistan. Yunnan Herbal Laboratory, College of Ecology and Environmental Sciences, Yunnan University, Kunming 650091, Yunnan, China (S. Bibi). Special Infectious Agents Unit, King Fahd Medical Research Centre, King Abdulaziz University, Jeddah, Saudi Arabia (E.I. Azhar).

E-mail addresses: shabana_bibi@ynu.edu.cn (S. Bibi), eazhar@kau.edu.sa (E.I. Azhar).

¹ Equal first author contribution: Shabana Bibi and Muhammad Saad Khan.

Peer review under responsibility of King Saud University.



1. Introduction

Viral infections are considerable threats for the public health. Severe acute respiratory syndrome coronavirus –2 (SARS-CoV-2) / COVID-19 is currently a critical human ailment spreading around the world. It appeared first in Wuhan city, China, in December 2019, which is famous for several kinds of international import and export (Bogoch et al., 2020; Lu et al., 2020). COVID-19 is badly affecting about two hundred countries around the globe (Hamdy M. Youssef et al., 2020), total reported cases 255,324,963 and the number of deaths are 5,127,696 by the current statistics until 19th November 2021 (Organization World Health, 2021).

SARS-CoV-2 is a single-stranded RNA-virus (29,891 bp), comprising 96% homology to bat coronavirus (CoV) whole genome sequence, and presented 79.6% sequence similarity with SARS-CoV

<https://doi.org/10.1016/j.jsps.2022.05.003>

1319-0164/© 2022 Published by Elsevier B.V. on behalf of King Saud University.

This is an open access article under the CC BY-NC-ND license (<http://creativecommons.org/licenses/by-nc-nd/4.0/>).

(Zhou et al., 2020). SARS-CoV-2 translates spike (S protein) - associated receptor domain which could interact to the human angiotensin-converting enzymes 2 (ACE-2) and encourages the fusion of membrane and approval of virus into cells for example in the lung by endocytosis (Corum and Zimmer, 2020; Ou et al., 2020; Yan et al., 2020; Zhou et al., 2020). When a virus enters the cells, just like other viruses SARS-CoV-2 also controlled the nucleic acid machinery and weaken the synthesis of new viral proteins, and also involves in the assembly of the proteins and therefore take control of viral replication (Chen et al., 2020).

The key viral proteins of SARS-CoV-2 are papain-like protease (PLpro), 3-chymotrypsin-like protease (3CLpro), spike S proteins and RNA-dependent RNA polymerase (Wu et al., 2020). The S protein able to bind with ACE-2, permitting the virus to move into host. Efforts are continuously being applied to repropose several promising antiviral drugs, therefore, hydroxychloroquine, chloroquine phosphate (Cortegiani et al., 2020), arbidol (Khamitov et al., 2008), lopinavir (Yao et al., 2020), and remdesivir (Holshue et al., 2020; Wang et al., 2020) have been tested and presented significant biological activities against SARS-CoV-2 infections. Current information of clinical trials of SARS-CoV-2 drugs is available in database "ClinicalTrials.gov" (Pang et al., 2020). Alternative medicine and traditional Chinese medicine have shown promising results for SAR-CoV-2 infection in China (Yang et al., 2020). Indeed, phytochemicals isolated from traditional plants are always of great importance for the management of several diseases (Patel et al., 2020; Suwannarach et al., 2020). With all previous effort, specific antiviral therapy for COVID-19 is still missing.

Bioinformatics and mathematical modeling have been conducted to hypothesized the methods/protocols to discover the dynamics of transmission of the COVID-19 in the human population, and suggest the strategies to control the multiplication of new cases in Saudi Arabia, and such kind of mathematical models could give the idea to work for the large dataset in future (Youssef et al., 2021, 2022; Hamdy M. Youssef et al., 2020; Hamdy M. Youssef et al., 2020). Structural modeling of repropose antiviral drugs has been the hot research topic after the emergence of COVID-19 (Bibi et al., 2022), because it's very important technique of drug design and discovery, these studies usually predict the importance of drug and target interaction, target with disease interactions, and drug with disease interactions, and ultimately significant to find out the potential treatments in less time (March-Vila et al., 2017). Integration of ligand-based (chemicals/drug-based) and structure-based (enzyme/protein based) methods has been studied in several drug design studies previously and hence proved its significance in drug discovery for many diseases (Bian et al., 2017; Honarparvar et al., 2014; Wilson and Lill, 2011). So that in this paper, an integrated drug design or computer-aided drug design approach (Bibi and Sakata, 2017a; Khan et al., 2021) was applied to selected chemical database for understanding the mechanism of protein–ligand interactions with the key residues, which could be helpful in finding potential natural main protease 3CLpro inhibitors with the significant activity to treat COVID-19.

2. Materials and methods

Several experimental attempts were made to investigate inhibitors against SARS-CoV-2 by utilizing various techniques explained in the previous literature (Bibi et al., 2021, 2020; Biswas et al., 2021). From different proteins of SARS-CoV-2 3CLpro is a unique target for identification of potential inhibitors as this protease is crucial for viral replication and therefore a promising target for drug (Anand et al., 2003; Mody et al., 2021). For inhibitors screening which could be further studied and developed as antivirals

compounds through enzymatic assay optimum conditions identification are necessary and that's conditions could be determined by biophysical and biochemical characterization of 3CLpro. Biochemical conditions data suggest that in the enzymatic assay of 3CLpro in the absence of salt basic pH or neutral conditions to be used (Ferreira and Rabeh, 2020). Results showed that against 3CLpro numerous natural products have shown encouraging inhibitory activities. Natural products like flavonoids (Park et al., 2016), terpenoids (J. Y. Park et al., 2012), diarylheptanoids (J.-Y. Park et al., 2012), and coumarins (Park et al., 2016) are potential inhibitors of the SARS-CoV proteases. By using the antiviral drugs database, computer-aided drug design (CADD) protocols were used to screen out potential SARS-CoV-2 3CLpro inhibitors (Fig. 1).

2.1. Construction of chemical database for in silico screening

Recent literature is available on the studies conducted to identify promising drugs for CoV infections (Chou et al., 2003; Farag et al., 2020; Hilgenfeld, 2014). Virtual screening techniques are highly recommended to find out the potential drugs for fatal and infectious diseases (Bibi and Sakata, 2016; Elmezayen et al., 2020; Jin et al., 2020a; Wang, 2020). An integrated CADD scheme has been employed using 78 natural compounds database to highlight the potential drug to combat COVID-19 infection. By utilizing the previous literature, botanical information, two-dimensional (2D) structures of selected 78 compounds along with the bioactivities for CoV infections have been enlisted in Table 1. The structure of each compound is drawn by using the ChemDraw software (Mills, 2006) and information of each structure was crosschecked from PubChem database (Kim et al., 2016) to reduce the chance of ambiguity and saved in SDF format for further analysis.

2.2. Selection of target protein

The selection of appropriate target protein for the drug design pipeline explains the important parameters necessary to clarify the action of bound ligands which could selectively inhibit the activity of 3CLpro to suppress the replication of SARS-CoV-2 activity in the host (Jin et al., 2020b). With PDB ID 6LU7, a target protein is selected to perform a molecular docking experiment in this study to evaluate the protein–ligand binding interactions (Jin et al., 2020b).

2.3. Molecular docking analysis

Molecular docking is an important CADD application for the identification of protein–ligand interactions to understand the molecular mechanism of small drug-like entities in cellular pathways (Bibi and Sakata, 2016; Khan et al., 2021). Information of selected 78 natural antiviral compounds used for molecular docking is presented in Table 1, and a three-dimensional (3D) structure of selected target protein is presented in Fig. 2. Target protein (PDB ID: 6LU7) in pdb format was imported to the MOE software (Vilar et al., 2008). Heteroatoms, 3D protonation, and water molecules along with the default ligand (N3) attached in the 3CLpro target protein were removed to prepare protein for the docking procedure shown in Fig. 2. An active site is identified in the selected 3CLpro selected protein (6LU7) which constitute the region among active domain I and II as shown in Fig. 2 and structural optimization is performed by following parameters; such as the addition of hydrogen atoms, energy minimization with respect to 0.1 gradients, MMFF94X force field, chiral constraints and geometrical parameter. By using the surfaces and maps panel module, transparency of the front and the back surface is adjusted and resulted in the information of significant residues in the selected substrate binding site of 6LU7 protein in the native conformation (Jin et al.,

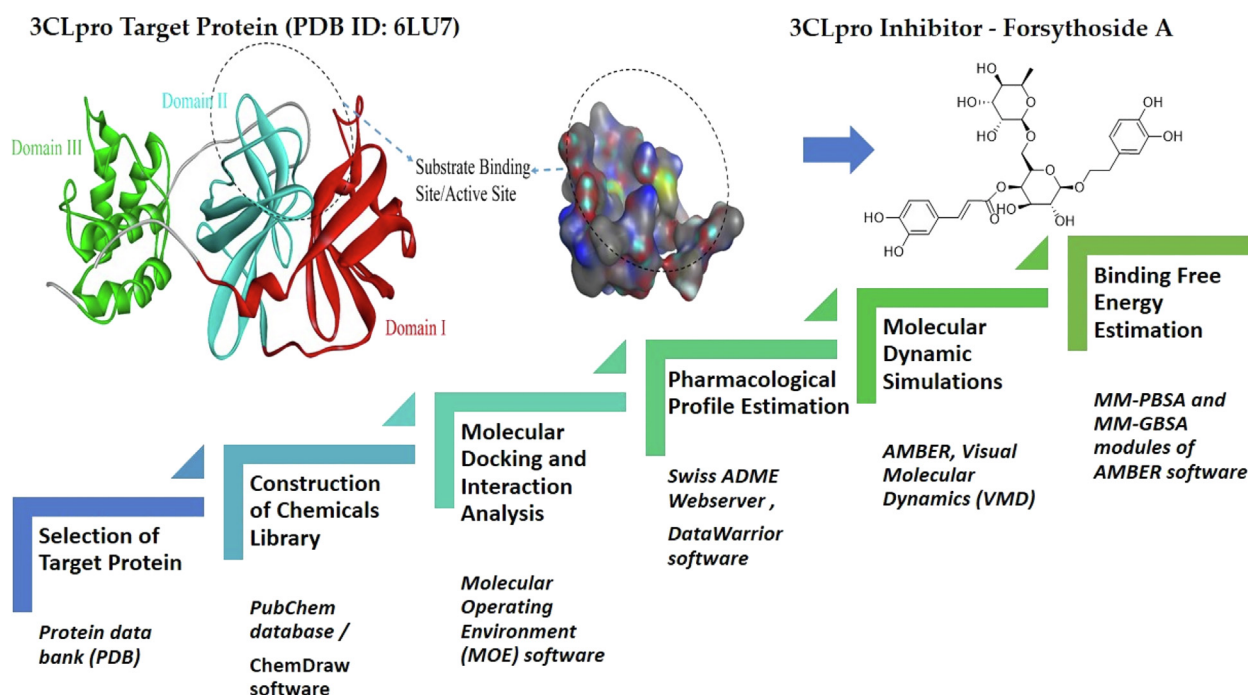


Fig. 1. Pipeline for screening of novel SARS-CoV-2 3CLpro inhibitors.

2020b; Naik et al., 2020). MOE software creates a database of natural 78 antiviral compounds collected from different reported studies to perform molecular docking simulations and saved with mdb extension for further analysis. Top-ranked poses are subjected for refinement and calculation of binding free energies (ΔG) which is evaluated by scoring function (GBVI/WSA dg) (Yousafi et al., 2020). A reliable scoring scheme that results in the docking score of the correct binding poses is established by a number of molecular interactions (hydrogen and hydrophobic interactions) (Aldeghi et al., 2016). MOE database of the docked complex was visualized carefully for understanding the mode of binding interactions of natural 3CLpro inhibitor bound in the selected pocket of the target protein.

2.4. Pharmacokinetic /ADMET profile estimation

The selected 10 top-scored compounds were used for the calculation of ADMET (absorption, distribution, metabolism, excretion, and toxicity) profile, and that is considered as an essential criterion for the drug-like screening of chemical compounds (Bibi and Sakata, 2017b; Fatima et al., 2018; Ntie-Kang et al., 2013). For the purpose of ADMET profile estimation of selected chemical compounds, SwissADME (Daina et al., 2014) and DataWarrior tools (Sander et al., 2015) were used.

2.5. Lead identification

An integrated drug design pipeline is designed in this study to identify the potential lead compound which could target 3CLpro for SARS-CoV-2 infections, 3CLpro is an acceptable target of CoV and have presented significance in blocking the viral replication and transcription procedure and becomes a striking therapeutic option for drug design of CoV infections (Hilgenfeld, 2014). The selected lead compound from the natural source presented significant results and fulfil maximum parameters of drug design, which includes biological activity, drug-likeness, pharmacokinetic profile, and best bounding to the active site residues of the protein, hence

limiting the virus replication and inactivate the main protease 3CLpro of SARS-CoV-2.

2.6. Molecular dynamics simulations

The lead compound complex was used for further MD simulation analysis at 100 ns to understand the behaviour of the docked complex and conformational stability in the system for practical applications. MD simulation protocols were divided into three major categories such as preparation of parameter files as input, followed by the pre-processing phase, and end with the simulation time-phase (Ahmad et al., 2019).

In the initial phase of file preparation, by the use of AMBER20's antechamber module (Lee et al., 2020), complex libraries with the parameters allied with 3CLPRO and Forsythoside A. In TIP3P solvation box, the complex system was solvated at 12 Å which was accomplished by the Leap module of AMBER. Molecular interactions were resolute by ff14SB force field (Case et al., 2014). For charge neutralization, Na^+ ions were added.

While in the pre-processing step of the system, the selected complex energies were improved by the numerous turns, completely established number of hydrogen atoms were abated for five hundred steps, minimization of system energy was recorded for thousand steps with limitation of two hundred kcal/mol – Å² on the residual arrangement, moreover, the minimization step was followed by the complete atoms minimization atleast once more for thousand steps with pragmatic restriction of five kcal/mol – Å² used for the system carbon alpha atoms, and three-hundred steps of minimization were applied for the system non-heavy atoms with the restriction of hundred kcal/mol – Å² on other system components. The complex was heated progressively to three-hundred K by NVT ensemble parameter, preserved by the Langevin dynamics (Izaguirre et al., 2001) and SHAKE algorithm (Krättiler et al., 2001) to confine the hydrogen bonding. The equilibration stage of the complex was retrieved at hundred-ps. The system pressure during the simulation period was maintained using NPT ensemble and limit the system to $C\alpha$ atoms of five kcal/mol – Å². The MD simulation plots of hundred-ns were generated using

Table 1
Selected dataset of 78 natural compounds that possess coronavirus activity.

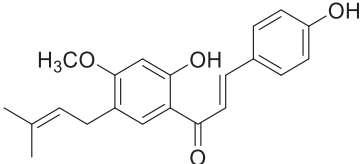
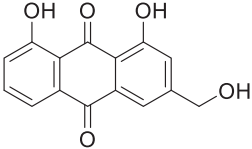
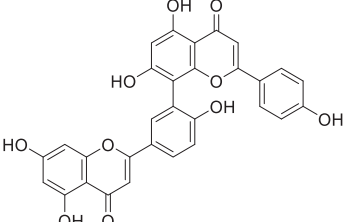
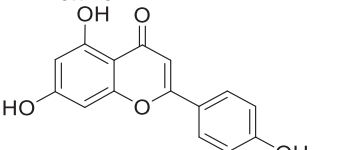
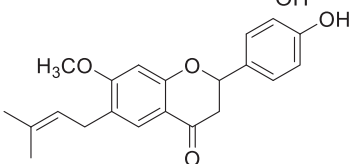
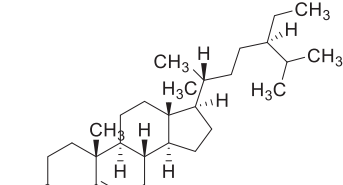
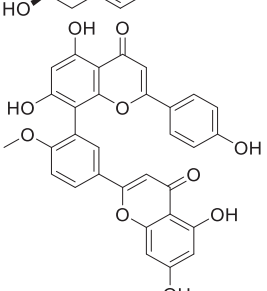
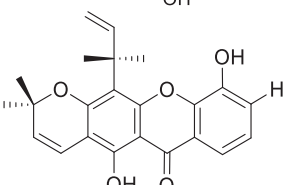
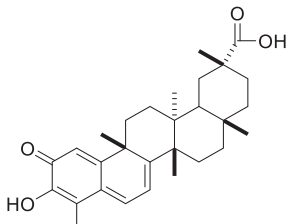
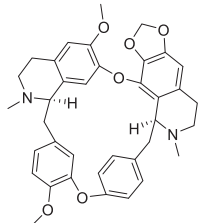
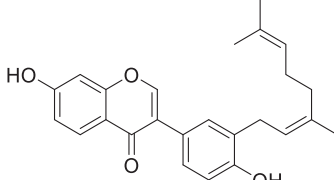
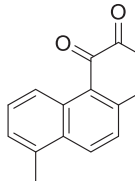
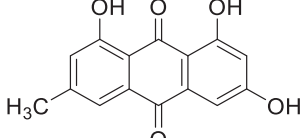
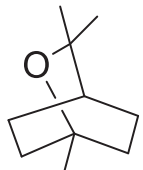
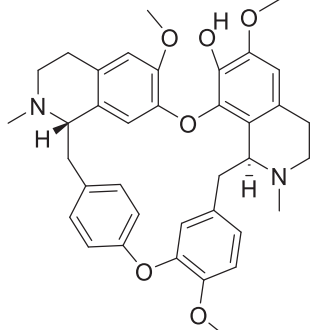
Compound	Chemical structure	CID	Source	Inhibitory constant (IC ₅₀ or EC ₅₀)	Ref
4'-O-methylbavachalcone		42607530	<i>Psoralea corylifolia</i>	10.1 μM	(Kim et al., 2014)
Aloe-emodin		10207	<i>Isatis indigotica</i>	8.3 μM	(Lin et al., 2005)
Amentoflavone		5281600	<i>Torreya nucifera</i>	8.3 μM	(Ryu et al., 2010)
Apigenin		5280443	<i>Houttuynia cordata</i>	0.4 μM	(Yin et al., 2011)
Bavachinin		10337211	<i>Psoralea corylifolia</i>	38.4 μM	(Kim et al., 2014)
Beta-sitosterol		222284	<i>Isatis indigotica</i>	1.210 μM	(Lin et al., 2005)
Bilobetin		5315459	<i>Torreya nucifera</i>	72.3 μM	(Ryu et al., 2010)
Blancoxanthone		11703574	<i>Calophyllum blancoi</i>	3 μM	(Shen et al., 2005)

Table 1 (continued)

Compound	Chemical structure	CID	Source	Inhibitory constant (IC ₅₀ or EC ₅₀)	Ref
Celastrol		122724	<i>Tritergium regelii</i>	10.3 μM	(Ryu et al., 2010)
Cepharanthine		10206	<i>Stephania tetrandra</i>	0.83 μM	(Kim et al., 2019)
Corylifol A		25056407	<i>Psoralea corylifolia</i>	32.3 μM	(Kim et al., 2014)
Dihydrotanshinone I		11425923	<i>Salvia miltiorrhiza</i>	14.4 μM	(J. Y. Park et al., 2012)
Emodin		3220	<i>Rheum officinale</i>	200 μM	(Ho et al., 2007)
Eucalyptol		2758	<i>Eucalyptus</i>	0.61 nM	(Sharma and Kaur, 2020)
Fangchinoline		73481	<i>Stephania tetrandra</i>	1.01 μM	(Kim et al., 2019)

(continued on next page)

Table 1 (continued)

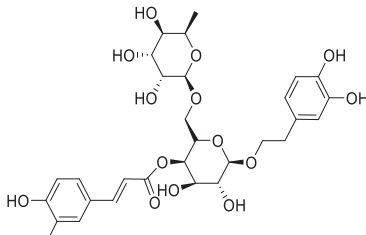
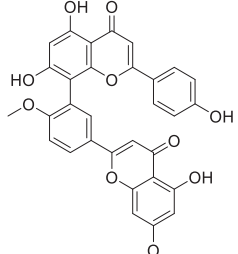
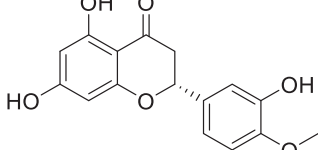
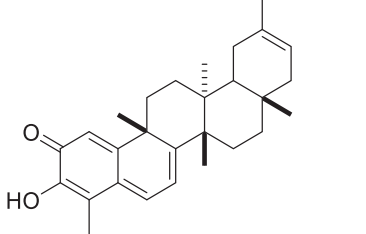
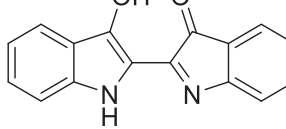
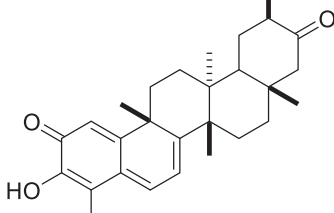
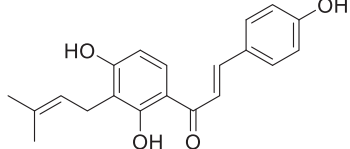
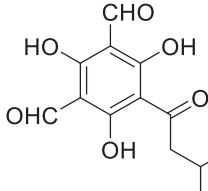
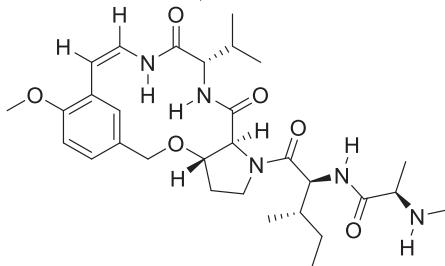
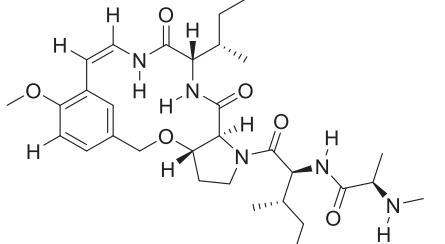
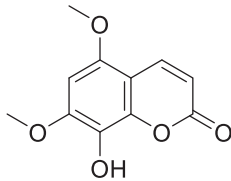
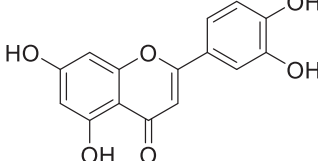
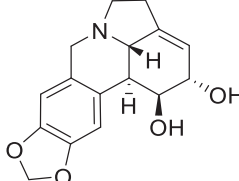
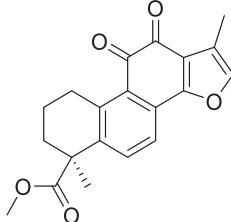
Compound	Chemical structure	CID	Source	Inhibitory constant (IC ₅₀ or EC ₅₀)	Ref
Forsythoside A		5281773	<i>Forsythia suspense</i>	0.64 mM	(Li et al., 2011)
Ginkgetin		5271805	<i>Torreya nucifera</i>	32.0 μM	(Ryu et al., 2010)
Hesperetin		72281	<i>Isatis indigotica</i>	365 μM	(Lin et al., 2005)
Igusterin		46881919	<i>Tritergium regelii</i>	2.6 μM	(Ryu et al., 2010)
Indigo		10215	<i>Isatis indigotica</i>	752 μM	(Lin et al., 2005)
Tingenone		101520	<i>Tritergium regelii</i>	9.9 μM	(Ryu et al., 2010)
Isobavachalcone		5281255	<i>Psoralea corylifolia</i>	7.3 μM	(Kim et al., 2014)

Table 1 (continued)

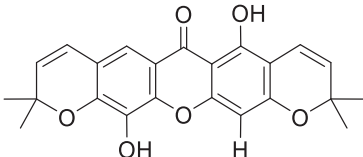
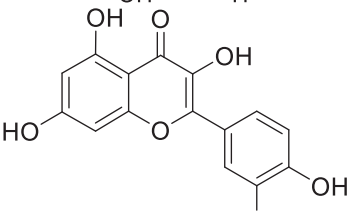
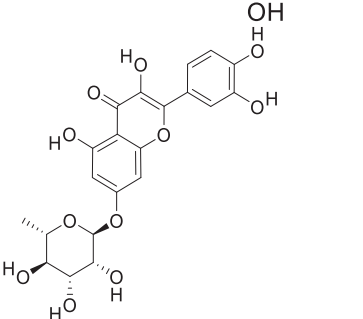
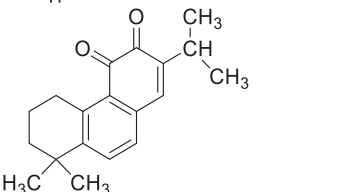
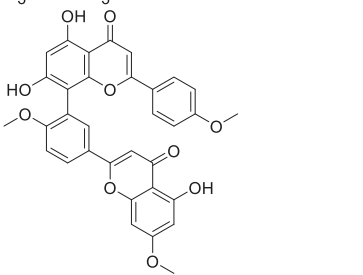
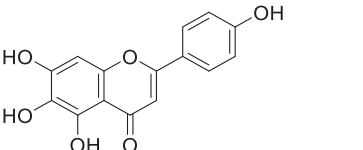
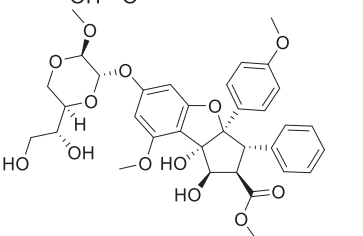
Compound	Chemical structure	CID	Source	Inhibitory constant (IC ₅₀ or EC ₅₀)	Ref
Jensenone		11594161	<i>Eucalyptus</i>	Not determined	(Yang et al., 2010)
Jubanine G		122216365	<i>Ziziphus jujuba</i>	13.41 μM	(Kang et al., 2015)
Jubanine H		122216366	<i>Ziziphus jujuba</i>	4.49 μM	(Kang et al., 2015)
Leptodactylone		442134	<i>Boenninghausenia sessilicarpa</i>	450 μM	(Yang et al., 2007)
Luteolin		5280445	<i>Galla chinensis</i>	10.6 μM	(Yi et al., 2004)
Lycorine		72378	<i>Lycoris radiata</i>	15.7 nM	(Li et al., 2005)
Methyl tanshinonate		14610613	<i>Salvia miltiorrhiza</i>	21.1 μM	(J. Y. Park et al., 2012))

(continued on next page)

Table 1 (continued)

Compound	Chemical structure	CID	Source	Inhibitory constant (IC ₅₀ or EC ₅₀)	Ref
Myricetin		5281672	<i>Scutellaria baicalensis</i>	2.71 μM	(Yu et al., 2012)
Neobavaisoflavone		5320053	<i>Psoralea corylifolia</i>	18.3 μM	(Kim et al., 2014)
Nummularine B		51017057	<i>Ziziphus jujuba</i>	6.17 μM	(Kang et al., 2015)
Pristimerin		159516	<i>Tritergium regelii</i>	5.5 μM	(Ryu et al., 2010)
Procyanidin A2		6325839	<i>Cinnamomi cortex</i>	29.9 μM	(Zhuang et al., 2009)
Procyanidin B1		11250133	<i>Cinnamomi cortex</i>	41.3 μM	(Zhuang et al., 2009)
Psoralidin		5281806	<i>Psoralea corylifolia</i>	4.2 μM	(Kim et al., 2014)

Table 1 (continued)

Compound	Chemical structure	CID	Source	Inhibitory constant (IC ₅₀ or EC ₅₀)	Ref
Pyranojacareubin		15307925	<i>Calophyllum blancoi</i>	15 μM	(Shen et al., 2005)
Quercetin		5280343	<i>Houttuynia cordata</i>	5.6 μM	(Yin et al., 2011)
Quercetin 7-rhamnoside		5748601	<i>Houttuynia cordata</i>	0.03 μM	(Yin et al., 2011)
Rosmariquinone		160142	<i>Salvia miltiorrhiza</i>	21.1 μM	(J. Y. Park et al., 2012))
Sciadopitysin		5281696	<i>Torreya nucifera</i>	38.4 μM	(Ryu et al., 2010)
Scutellarein		5281697	<i>Scutellaria baicalensis</i>	0.86 μM	(Yu et al., 2012)
Silvestrol		11787114	<i>Aglaia foveolata</i>	1.3 μM	(Müller et al., 2018)

(continued on next page)

Table 1 (continued)

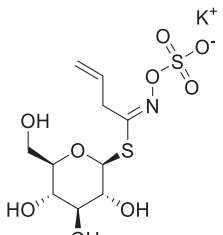
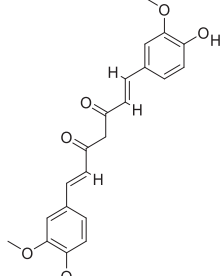
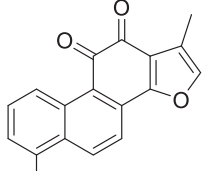
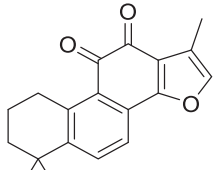
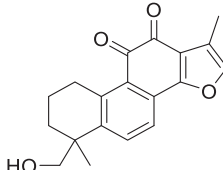
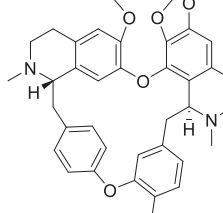
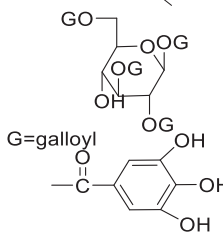
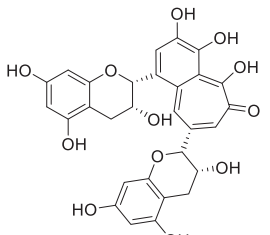
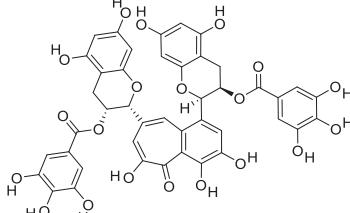
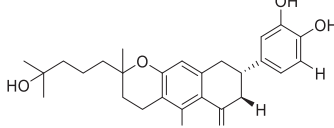
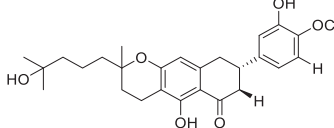
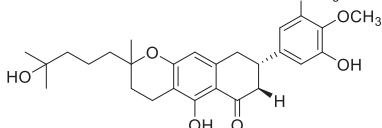
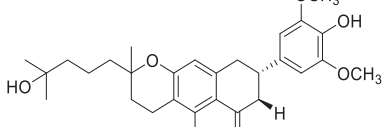
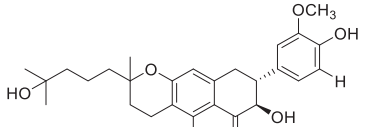
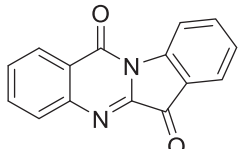
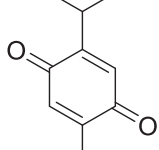
Compound	Chemical structure	CID	Source	Inhibitory constant (IC ₅₀ or EC ₅₀)	Ref
Sinigrin		6911854	<i>Isatis indigotica</i>	217 μM	(Lin et al., 2005)
Curcumin		969516	<i>Curcuma longa</i>	0.2 μM	(J. Sharifi-Rad et al., 2020)
Tanshinone I		114917	<i>Salvia miltiorrhiza</i>	38.7 μM	(J. Y. Park et al., 2012))
Tanshinone IIA		164676	<i>Salvia miltiorrhiza</i>	89.1 μM	(J. Y. Park et al., 2012))
Tanshinone IIB		318797	<i>Salvia miltiorrhiza</i>	24.8 μM	(J. Y. Park et al., 2012))
Tetrandrine		73078	<i>Stephania tetrandra</i>	0.33 μM	(Kim et al., 2019)
Tetra-O-galloyl-D-glucose		5153644	<i>Galla chinensis</i>	4.5 μM	(Yi et al., 2004)

Table 1 (continued)

Compound	Chemical structure	CID	Source	Inhibitory constant (IC ₅₀ or EC ₅₀)	Ref
Theaflavin monogallates		169167	<i>Camellia sinensis</i> (black tea)	Not determined	(Lung et al., 2020)
Theaflavin 3,3'-digallate		135403795	<i>Camellia sinensis</i> (black tea)	9.5 μM	(Chen et al., 2005)
Tomentin A		71659627	<i>Paulownia tomentosa</i>	6.2 μM	(Cho et al., 2013)
Tomentin B		71659628	<i>Paulownia tomentosa</i>	6.1 μM	(Cho et al., 2013)
Tomentin C		71659765	<i>Paulownia tomentosa</i>	11.6 μM	(Cho et al., 2013)
Tomentin D		71659766	<i>Paulownia tomentosa</i>	12.5 μM	(Cho et al., 2013)
Tomentin E		71659767	<i>Paulownia tomentosa</i>	5.0 μM	(Cho et al., 2013)
Tryptanthrin		73549	<i>Strobilanthes cusia</i>	0.06 μg/mL	(Tsai et al., 2020)
Thymoquinone		10281	<i>Nigella sativa</i>	0.3 μM	(Srinivasan, 2018)

(continued on next page)

Table 1 (continued)

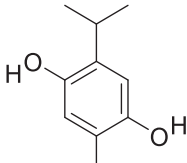
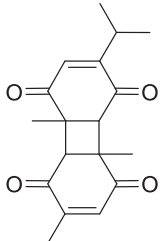
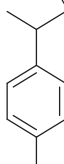
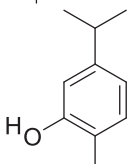
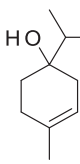
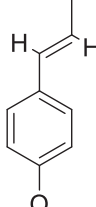
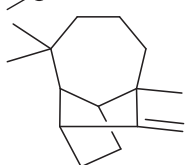
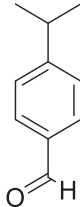
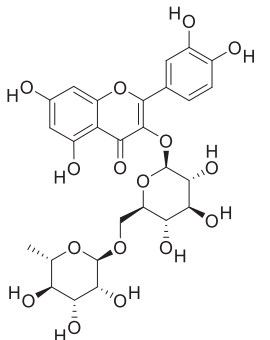
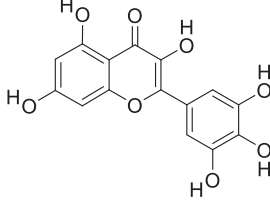
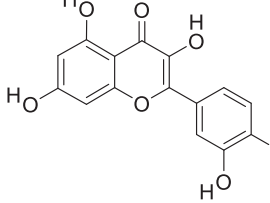
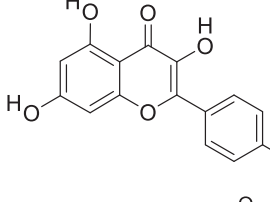
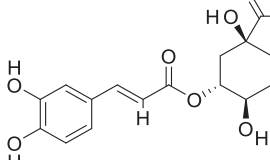
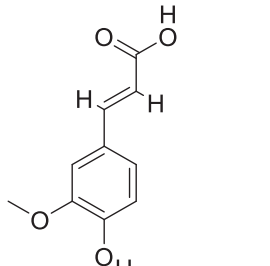
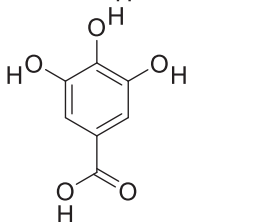
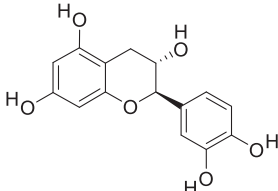
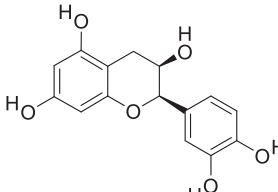
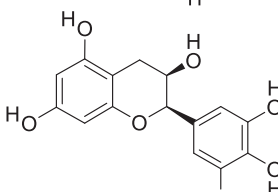
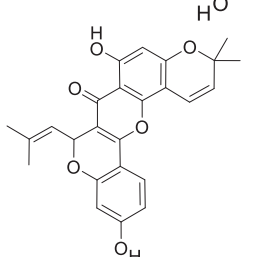
Compound	Chemical structure	CID	Source	Inhibitory constant (IC ₅₀ or EC ₅₀)	Ref
Thymohydroquinone		95779	<i>Nigella sativa</i>	3.1 μM	(Srinivasan, 2018)
Dithymoquinone		398941	<i>Nigella sativa</i>	Not determined	(Srinivasan, 2018)
P-CYMENE		7463	<i>Nigella sativa</i>	0.4354 μM	(Srinivasan, 2018)
Carvacrol		10364	<i>Nigella sativa</i>	1.06 μM	(Srinivasan, 2018)
Terpinen-4-ol		11230	<i>Nigella sativa</i>	30 μM	(Srinivasan, 2018)
Anethole		637563	<i>Nigella sativa</i>	4650 μM	(Srinivasan, 2018)
Longifolene		289151	<i>Nigella sativa</i>	Not determined	(Srinivasan, 2018)
Cuminaldehyde		326	<i>Cuminum cyminum</i>	50 μM	(Srinivasan, 2018)

Table 1 (continued)

Compound	Chemical structure	CID	Source	Inhibitory constant (IC ₅₀ or EC ₅₀)	Ref
Rutin		5280805	<i>Morus nigra</i>	0.012 μM	(Tokusoglu, 2016)
Myricetin		5281672	<i>Morus nigra</i>	0.012 μM	(Tokusoglu, 2016)
Quercetin		5280343	<i>Morus nigra</i>	0.00011 μM	(Tokusoglu, 2016)
Kaempferol		5280863	<i>Morus nigra</i>	0.028 μM	(Tokusoglu, 2016)
Chlorogenic acid		1794427	<i>Morus nigra</i>	0.2 μM	(Tokusoglu, 2016)
Ferulic acid		445858	<i>Morus nigra</i>	0.2 μM	(Tokusoglu, 2016)
Gallic acid		370	<i>Morus nigra</i>	0.06 μM	(Tokusoglu, 2016)

(continued on next page)

Table 1 (continued)

Compound	Chemical structure	CID	Source	Inhibitory constant (IC ₅₀ or EC ⁵⁰)	Ref
(+)-catechin		9064	<i>Morus nigra</i>	1.61 μM	(Tokusoglu, 2016)
(-)-Epicatechin		72276	<i>Morus nigra</i>	0.407 μM	(Tokusoglu, 2016)
Epigallocatechin		72277	<i>Morus nigra</i>	0.48 μM	(Tokusoglu, 2016)
Cyclomorusin		5481969	<i>Morus nigra</i>	1.7 μM	(Tokusoglu, 2016)

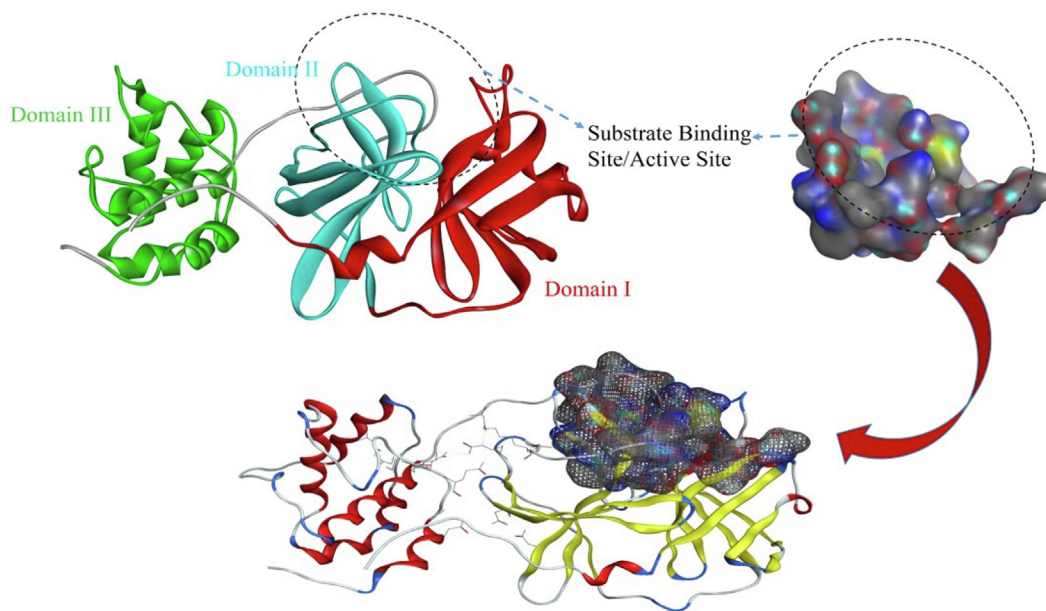


Fig. 2. Structural representation of selected target protein 3-chymotrypsin-like protease (3CLpro) PDB ID: 6LU7 presented with the identified domains and target protein active site (structure covered by black net) by molecular operating environment (MOE) software.

a time scale of two-fs. Bounded and unbounded interactions analyses were performed by keeping the limiting distance of eight-Å. CPPTRAJ module (Roe and Cheatham, 2013) was cast-off at the end to do the statistical calculation for multiple structural considerations to enquire stability of the lead complex selected complex. Visual molecular dynamic (VMD) tool is used for the MD simulation trajectories (Humphrey et al., 1996).

2.7. Binding free energy (BFE) estimation

The interaction energy and solvation free energy for the selected 3CL_{PRO} receptor, Forsythoside A, 3CL_{PRO}- Forsythoside A complex were estimated by using the significant module of MMPBSA.py (Miller et al., 2012) of software AMBER20. Moreover, it is reported that an average value of the system was recorded as gross BFE of the system. The BFE was calculated with MM-PBSA module and its corresponding MM-GBSA calculations of AMBER modules with aims to develop the difference between the bound and unbound presentation of solvated conformations of the same molecule (Humphrey et al., 1996). Mathematically, the BFE can be calculated through Eq. (1),

$$\Delta G_{\text{bind,solv}} = \Delta G_{\text{bind,vacuum}} + \Delta G_{\text{solv, 3CL}_{\text{PRO}} - \text{Forsythoside A}} - (\Delta G_{\text{solv, Forsythoside A}} + \Delta G_{\text{solv, 3CL}_{\text{PRO}}}) \quad (1)$$

For all three states of the system, the solvation energy was estimated by resolving either Poisson Boltzmann (PB) or Generalized Born (GB) equation and thus it will give the electrostatic role of the solvation state. It also permits the calculation of empirical terms for hydrophobic assistances as shown in Eq. (2).

$$\Delta G_{\text{solv}} = G_{\text{electrostatic, } \epsilon=80} - G_{\text{electrostatic, } \epsilon=1} + \Delta G_{\text{hydrophobic}} \quad (2)$$

Calculation of the average interaction energy between 3CL_{PRO} and Forsythoside A gives to delta- ΔG_{vacuum} (Eq. (3)).

$$\Delta G_{\text{vacuum}} = \Delta E_{\text{molecular mechanics}} - T.\Delta S \quad (3)$$

3. Results

3.1. Database of selected natural compounds

Reported natural antiviral compounds isolated from different plant species were used to generate a database by MOE software (Vilar et al., 2008; Yousafi et al., 2020). 78 compounds with their chemical structures, PubChem identifier (CID), botanical information, and inhibitory constant values with respect to antiviral studies including SARS-CoV and MERS-CoV infections also are enlisted in Table 1. Each compound has been studied for anti-viral diseases and blocked virus entry into the host, virus replication, and translation activities. Therefore, in this study, computational techniques have been used to screen anti-SAR-CoV-2 3CLpro drugs, which could bind significantly within the substrate-binding pocket.

3.2. Protein-ligand interaction analysis

The most important step in CADD is molecular docking performed by MOE software (Vilar et al., 2008), ligand and protein structure are the preliminary requirement to start the molecular docking procedure so the previous knowledge of target protein is utilized, 3CLpro is a molecular target for the development of anti-COVID-19 drug (Hilgenfeld, 2014; Wu et al., 2020). The 3D structural information of the 3CLpro enzyme (PDB ID: 6LU7) has been used. The prepared enzyme/protein structure without any bounded ligand and considerable substrate-binding active site for the molecular docking and

interaction analysis was identified from literature (Jin et al., 2020b) as shown in Fig. 2.

Database of 78 natural compounds generated by MOE with.mdb extension was docked in the same active site by Dock module of MOE software (Vilar et al., 2008), lead compound "Forsythoside A" with the best binding poses, and molecular interactions with the significant amino acids intricate the mechanism of inhibition of 3CLpro for SARS-CoV-2 infections are presented graphically in Fig. 3. Thr26 (A), Cys145 (A), Met165 (A), and Glu166 (A) are the key amino acids that play role in the hydrogen bonding interactions between the lead compound and the selected active binding pocket of 3CLpro.

By the evaluation of selected active binding site following residues (Thr24 (A), Thr25 (A), Thr26 (A), His41 (A), Met49 (A), Tyr54 (A), Phe140 (A), Leu141 (A), Asn142 (A), Gly143(A), Ser144 (A), Cys145 (A), His163 (A), His164 (A), Met165 (A), Glu166 (A), Leu167(A), Pro168 (A), His172 (A), Asp187 (A), Arg188 (A), Aln189 (A), Thr190(A), Ala191(A), Gln192(A)) were highlighted for significant activity (Jin et al., 2020b; Naik et al., 2020). Table 2 describes the summary of molecular docking analyses of selected top 10 compounds. Selected ten compounds have demonstrated the best binding poses with the highest dock score within the range of -8.6628 to -7.8328. All compounds have demonstrated a significant docked score along with the number of hydrogen bonds (HBs) within the range of 4.5 Å.

Compound 1 "Jubanine H" and Compound 2 "Forsythoside A" have presented very good docking results above threshold hold values of acceptable dock score which is -8.0 Kcal/mol and also presented significant binding interactions with the key amino acid residues of the active site of the target protein. Moreover, top scored six compounds enlisted in Table 2 have presented good energy value above -8.0 Kcal/mol and binding interactions with significant residues of substrate binding active site of the selected 3CLpro target enzyme.

3.3. Pharmacokinetic /ADMET profile estimation

Several studies have proved the importance of pharmacokinetic / ADMET profile estimation for the screening of databases to identify potential drug-like and a lead-like compounds that could be better tolerable in the design and development of new drugs (Bibi and Sakata, 2017b; Ntie-Kang et al., 2013; Sepay et al., 2020). ADMET properties are calculated by SwissADME (Daina et al., 2017) and Datawarrior tools (Sander et al., 2015). Physico-chemical properties of the selected 10 compounds, such as partition coefficient/ lipophilic parameters (logP values), hydrogen bond acceptor (HBA), hydrogen bond donor (HDB), total polar surface area (TPSA), molar refractivity (MR), and rotatable bond (RB) were calculated for each compound. As initial phase drug discovery protocols promote the calculation of drug-likeness, water-solubility, pharmacokinetics, toxicity estimations along with the medicinal chemistry perspective as mentioned for top-scored ten compounds in Table 3.

Due to the large chemical structure of natural compounds in the selected dataset, physicochemical properties described by Lipinski (Lipinski et al., 1997) and Veber's (Veber et al., 2002) in the theory of drug-likeness are violating one or more parameters shown in Table 3. The lipophilic profile and water solubility of the selected ten compounds are moderate or quite low values. Toxicity estimation of 10 selected compounds presented significant results in the form of mutagenic, tumorigenic, reproductive and irritant effects while four compounds showed minor violations. Five compounds have presented no alerts in the medicinal chemistry parameter evaluation while five compounds have presented one or two alerts. The pharmacokinetic properties of selected 10 compounds vary with respect to other

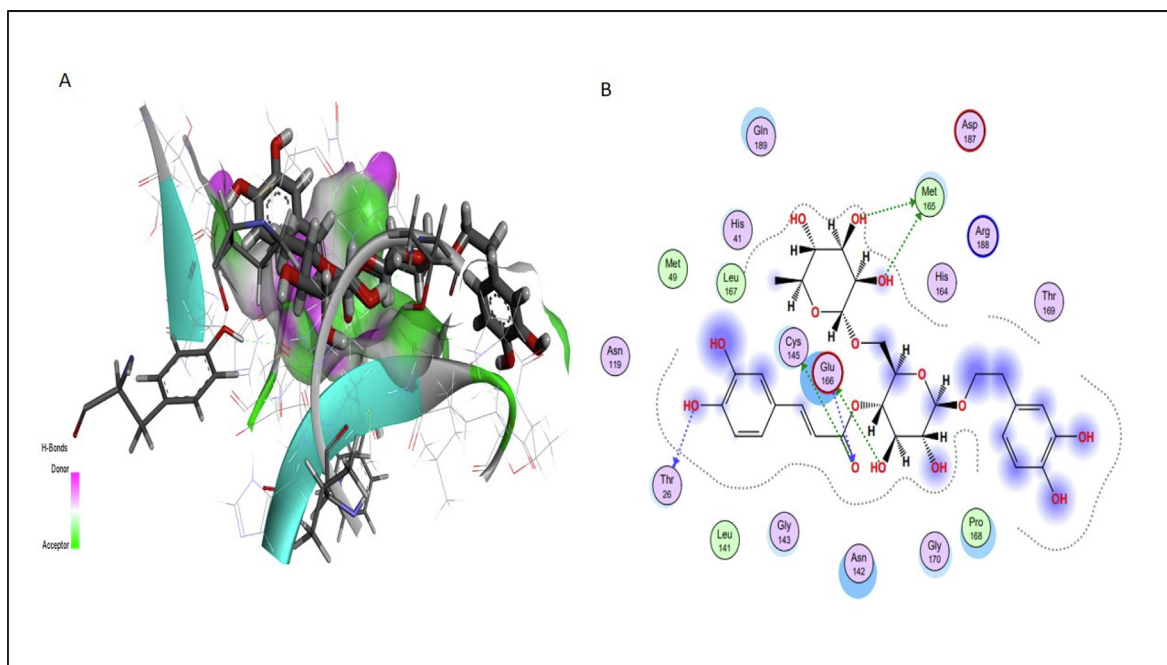


Fig. 3. Schematic representation of lead compound "Forsythoside A" in the active site of 3-chymotrypsin-like protease-3CLpro target protein. Three-dimensional view of the interacting hydrogen-bonded surface area in target active site [A], Two-dimensional plot of interacting residues showing best hydrogen bonding interactions and other important hydrophobic interacting residues [B].

Table 2

Summary of molecular docking analyses of top scored 10 compounds.

Sr #	Name of Compound	CID	Dock Score	Interacting residues in the binding pocket				
				Ligand	Receptor	Interaction	Distance	E (kcal/mol)
1	Jubanine H	122216366	-8.6628	O2	SG:Cys145(A)	H-donor	3.02	-3.5
				O5	SG:Cys145(A)	H-donor	3.82	-0.6
				N8	O:Glu166(A)	H-donor	3.11	-3.9
				C17	SG:Cys145(A)	H-donor	3.40	-0.9
				C31	SD:Met49(A)	H-donor	3.37	-0.5
2	Forsythoside A	5281773	-8.6225	O6	OE2:Glu166(A)	H-donor	2.74	-2.4
				O8	SD:Met165(A)	H-donor	3.75	-1.1
				O9	SD:Met165(A)	H-donor	3.46	-1.3
				O11	SG:Cys145(A)	H-donor	3.90	-1.2
				O15	O:Thr26(A)	H-donor	2.94	-3.7
				O11	N:Glu166(A)	H-acceptor	3.07	-3.4
				O8	SG:Cys145(A)	H-donor	3.36	-0.9
3	Theaflavin 3,3'-digallate	135403795	-8.4503	C16	O:Thr26(A)	H-donor	2.92	-2.6
				C19	O:Thr26(A)	H-donor	2.88	-1.9
				C17	SG:Cys145(A)	H-donor	3.81	-0.6
4	Jubanine G	122216365	-8.3639	O4	N:Gly143(A)	H-acceptor	2.99	-4.2
				O2	SG:Cys145(A)	H-donor	3.37	-1.0
5	Silvestrol	11787114	-8.1613	O13	OD1:Asn119(A)	H-donor	2.96	-1.7
				O17	SG:Cys145(A)	H-donor	3.58	-0.8
				O6	CB:Met165(A)	H-acceptor	3.14	-0.5
				6-ring	CA:Gln189(A)	H-pi	3.79	-1.7
				N10	OG1:Thr25(A)	H-donor	3.19	-1.1
6	Nummularine B	51017057	-8.0029	C14	OD1:Asn142(A)	H-donor	3.14	-0.6
				O3	NE2:Gln189(A)	H-acceptor	2.81	-0.6
				6-ring	CA-Gln189(A)	H-pi	4.15	-0.8
				6-ring	N:Thr26(A)	H-pi	4.68	-0.6
7	Tetrandrine	73078	-7.9691	O11	OD1:Asn142(A)	H-donor	2.95	-0.5
8	Beta-sitosterol	222284	-	O5	O:Arg188(A)	H-donor	2.81	-2.1
9	Theaflavin monogallates	169167	-7.8981	O9	OG:Ser46(A)	H-acceptor	2.83	-0.7
10	Ginkgetin	5271805	-7.8328	6-ring	CG2:Thr25(A)	H-pi	3.82	-0.5
				6-ring	N:Thr26(A)	H-pi	4.68	-0.6

drug-like parameters because most of the plant-derived compounds don't fulfil the Lipinski rule of drug-likeness due to their large chemical structures (Katiyar et al., 2012; Yousafi et al., 2020).

3.4. Lead identification

Out of ten selected compounds based on top dock scores. It is hard to select a lead compound with all acceptable ADMET

Table 3
Summary of pharmacokinetic/ADMET properties of 10 selected compounds.

ADMET properties	Jubanine H	Forsythoside A	Theaflavin 3,3'-digallate	Jubanine G	Silvestrol	Nummularine B	Tetrandrine	Beta-sitosterol	Theaflavin monogallates	Ginkgetin
Physicochemical Properties										
MW	585.73	624.59	868.70	571.71	654.66	591.70	622.75	414.71	716.60	566.51
RB	11	11	8	10	11	10	4	6	5	5
HBA	7	15	20	7	13	7	8	1	16	10
HBD	4	9	13	4	4	4	0	1	11	4
MR	172.44	148.42	215.39	167.64	161.84	173.34	186.07	133.23	179.69	155.91
TPSA	138.10	245.42	351.12	138.10	171.83	138.10	61.86	20.23	284.36	159.80
B.S	0.17	0.17	0.17	0.17	0.17	0.17	0.55	0.55	0.17	0.55
Lipophilicity										
LogP _{o/w} (iLOGP)	4.39	2.41	0.73	2.23	4.35	3.16	4.87	4.79	1.75	3.94
LogP _{o/w} (XLOGP3)	2.89	-0.50	4.71	2.53	1.64	3.12	6.66	9.34	1.79	5.69
LogP _{o/w} (WLOGP)	0.55	-1.12	3.53	0.16	1.36	0.37	5.75	8.02	2.55	5.74
Consensus LogP _{o/w}	2.10	-0.55	1.86	1.40	1.94	1.86	5.41	7.19	1.33	4.34
Water solubility Class										
Class	Moderately soluble	Soluble	Moderately soluble	Moderately soluble	Moderately soluble	Moderately soluble	Insoluble	Poorly soluble	Moderately soluble	Poorly soluble
Pharmacokinetics										
BBB permeability	No	No	No	No	No	No	No	No	No	No
GI absorption	High	Low	Low	High	Low	High	High	Low	Low	Low
CYP1A2 inhibitor	No	No	No	No	No	No	No	No	No	No
P-gp substrate	Yes	Yes	Yes	Yes	Yes	Yes	No	No	No	No
CYP2C19 inhibitor	No	No	No	No	No	No	No	No	No	No
CYP2C9 inhibitor	No	No	Yes	No	No	No	No	No	Yes	Yes
CYP2D6 inhibitor	No	No	No	No	No	No	No	No	No	No
CYP3A4 inhibitor	Yes	No	No	Yes	Yes	Yes	No	No	No	No
Log Kp (Skin permeation)	-7.82	-10.46	-8.25	-7.99	-9.13	-7.69	-5.37	-2.20	-9.40	-5.72
Toxicity estimation										
Mutagenic	None	None	None	None	None	None	None	None	Low	None
Tumorigenic	None	None	None	None	None	None	None	None	None	None
Reproductive effects	None	None	None	None	High	None	None	None	None	None
Irritant effects	Low	None	None	Low	None	Low	None	None	None	None
Medicinal Chemistry										
PAINS	No alert	1 alert	1 alert	No alert	No alert	No alert	No alert	No alert	1 alert	No alert
Brenk	No alert	2 alert	2 alert	No alert	No alert	No alert	No alert	1 alert	1 alert	No alert
Synthetic accessibility	7.38	6.37	6.36	7.17	6.60	6.93	7.01	6.30	5.80	4.50

parameters until it is tested to formulate the final activity and dose of the selected drug. Because these are natural compounds in the selected dataset having large chemical structures, So ADMET parameters usually violate but as the molecular docking results are promising, the selected lead compound have generated 6 HBs and very notable binding energy (-8.6225 kcal/mol) and presented interacts with the significant residues of the active site (Fig. 3). Lead compound's medicinal status is confirmed from the literature also and founds effective with respect to potential anti-viral drugs for avian infections of bronchitis virus (Li et al., 2011; Wang et al., 2021), influenza virus (Law et al., 2017), and CoV (Bailly, 2021). Some recent studies highlight the importance of our selected lead compound "Forsythoside A" an active chemical isolated from *Forsythia suspense* and famous for different pharmacological activities and most commonly used traditional antiviral medicine (Bailly, 2021). While in this integrated drug design study, Forsythoside A has presented significant biochemical and structural activity as 3CLpro inhibitor for SARS-CoV-2 infections.

3.5. Molecular dynamics simulations

To validate the structural behaviour of lead compounds within the substrate-binding active cavity of 3CLpro was used to run MD simulations at 100 ns. 3CLpro protein stability is the description of all the net forces to determine whether the protein will remain in folded state or assume non-native congregating structures. Superimposition of 3CLpro at 0 ns and 100 ns is demonstrated in Fig. 4. Therefore, comparing the protein–ligand complexes conformation at a different level of stimulation until 100 ns provides highly useful structural insights that help to understand the possible changes in the ligand pose generated as a result. Hence, a RMSD of 1.303 Å was noted during complex comparison at 0 ns (tan colour) and 100 ns (blue colour) simulation, which indicates minor divergence in the structural conformation due to movement in ligand pose depicted in Fig. 4.

During the simulation, 2D plots were generated to explain the fluctuating behaviour of the docked complex at different time frames during MD simulation productions. These plots are important for the MD simulations statistical analysis, hence it could be significant to decode the backbone stability and flexibility of the residues during the different time frames of MD simulations (Ismail et al., 2020). Results show that the RMSD calculates the small atoms convergence from a reference state (Fig. 5A), while

the RMSF of a protein explained the protein's dynamic nature that contributed to the system's overall versatility and residual mobility from its mean position (Fig. 5B). It is noted that the average RMSD value was 2.21 Å and the average RMSF value was 1.14 Å for the complex of Forsythoside A drug with 3CLpro target protein and almost similar residues were involved in the binding interactions at 0 ns and 100 ns, which seems maximum correlation with the docking results, and minor fluctuations of the 3CLpro protein residues were observed from the initial state during MD simulation runs.

The radius of gyration (Rg) was evaluated to confirm the compactness and equilibrium conformation of the system, it is expected that the high and low values of radius of gyration describe the magnitude of system compactness and system less tight packing. It also explains the system of concern if the weather is in order or not as required. A high compact system encourages MD simulations system stability. The estimated average Rg of the system was 22.70 Å with the maximum value of 38.45 Å at 19.19 ns reflecting the higher-ordered and compact nature of the system (Fig. 6A). The thermal residual deviation was assessed afterwards by beta-factor (BF) (Fig. 6B), therefore the results seem effectively correlated with RMSF and hereafter approves the stability of the system. BF and RMSF are complemented each other in terms of overall system stability and residual flexibility. The average BF of the system analyzed is 39.56 Å with a maximum of 346.31 Å.

The frequency of the HBs in each time frame of the MD simulation plots can be visualized in Fig. 7A. Hydrogen bonding plays an important role in overall complex stability, an increase in HBs increases the binding affinity of the drug molecule for the protein binding site and thus strengthen the complex stability. These HBs were extracted by means of VMD hydrogen bond plugin. The estimated maximum number of HBs between SARS-CoV-2 3CLpro residues and Forsythoside A atom were 2 and the minimum number of HBs was 1 respectively during MD simulation analysis until 0–100 ns. Solvent accessible surface area (SASA) that explains the thermodynamic stability of the protein was also calculated through the MD simulation run. SASA is a very useful analysis in which changes in the accessibility of the protein to solvent can be determined. A high peak of 157 nm² was observed at 30 ns and later stabilized with an average value of accessibility 151.42 nm² in Fig. 7B.

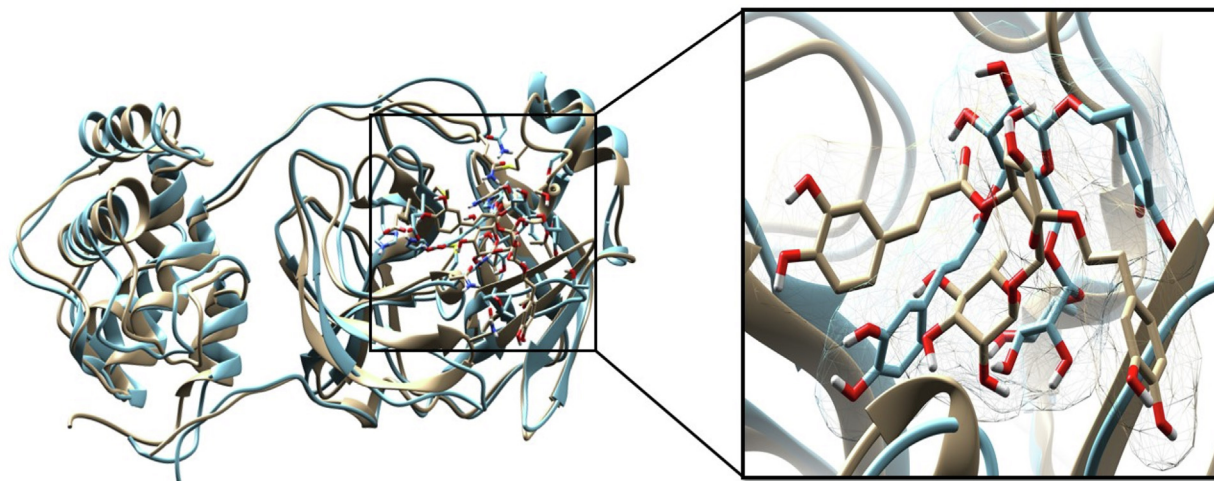


Fig. 4. Superimposition of 3CLpro complex with "Forsythoside A" at 0 ns and 100 ns. The calculated RMSD value is 1.303, complex at 0 ns is presented in a tan colour and 100 ns is presented in blue colour. Critical structural changes are shown in zoomed view.

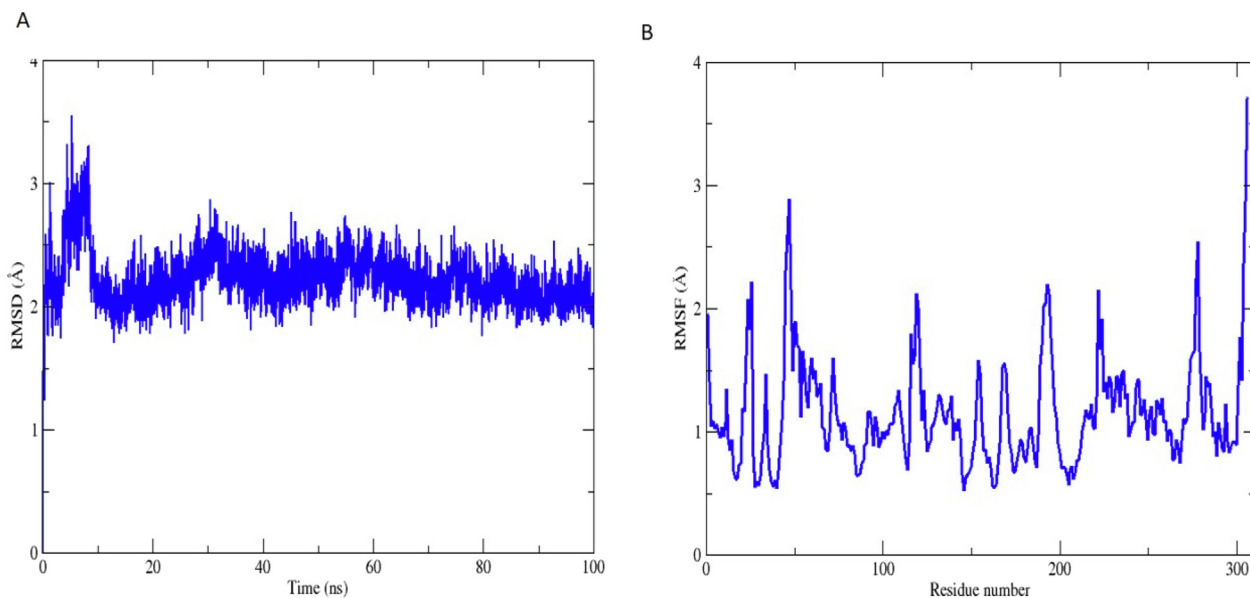


Fig. 5. Root mean square deviation (RMSD) value of 3CLpro-inhibitor complex until 0–100 ns [A]. Y-axis is showing the RMSD calculations in Angstrom (Å) while X-axis is showing the variation of bonded conformation through time in nanoseconds (ns). Root Mean Square Fluctuation (RMSF) of 3CLpro protein [B]. Y-axis is showing the RMSF calculations in Angstrom (Å) while X-axis is showing the index of the residue during 0–100 ns simulation time span.

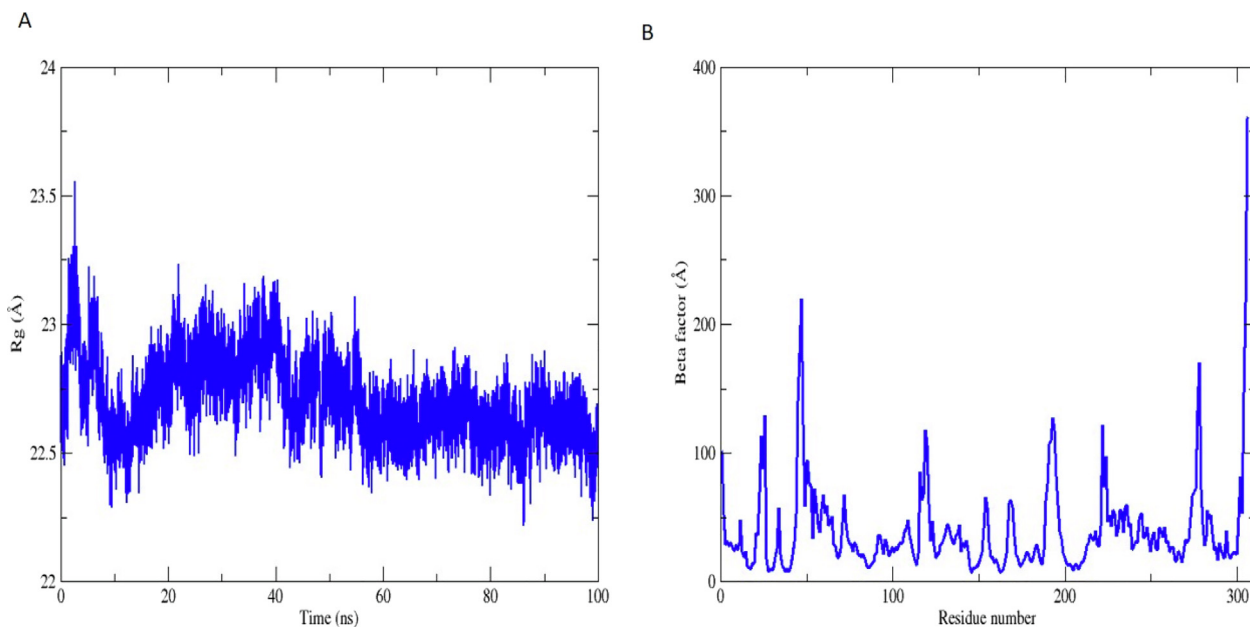


Fig. 6. Radius of gyration (Rg) value of 3CLpro-inhibitor complex until 0–100 ns [A]. Y-axis is showing the Rg calculations in Angstrom (Å) while X-axis is showing the variation of bonded conformation through time in 0–100 ns (ns). The beta factor of 3CLpro protein [B]. Y-axis is showing the beta factor calculations in Angstrom (Å) while X-axis is showing the index of the residue during 0–100 ns simulation time span.

3.6. Binding free energies (BFE) calculations

The understanding of net BFE or total energy (ΔT energy) of the moelcues in both simulation models is important to describe the favourable receptor - ligand bounded complex in biomolecluar modeling. In the explicit solvent system, the net BEF for the 3CLpro - Forsythoside A bounded complex is -40.0981 kcal/mol (GB model) and -36.5514 kcal/mol (PB model), respectively. Special emphasis is for GB model and PB model based energy estimations during 100 ns MD simulation run, the estimated gas energy for the system is noticed as -116.2404 kcal/mol for GB model, hereafter for PB model, gas energy is noticed as -116.2404 kcal/mol that also

the same value without any noticeable difference. Solvation free energy in the case of GB is 76.1423 kcal/mol while in the case of PB it is 79.6891 kcal/mol.

The electrostatic impact to the system assessed by molecular mechanics (MM) force field is very much acceptable to the net energy as -76.8056 kcal/mol. Similarly, the Van der Waals impact from MM also associated with the system stability estimated as -39.4349 kcal/mol. The electrostatic energy impact (presented as EGB and EPB) to the ΔG solvation energy is considerable factor focussed to a non-acceptable impact in GB solvation energy. The surface area energy (ESURF) estimated is -5.3735 kcal/mol for GB model. In PB, ENPOLAR and EDISPER are the repellent and

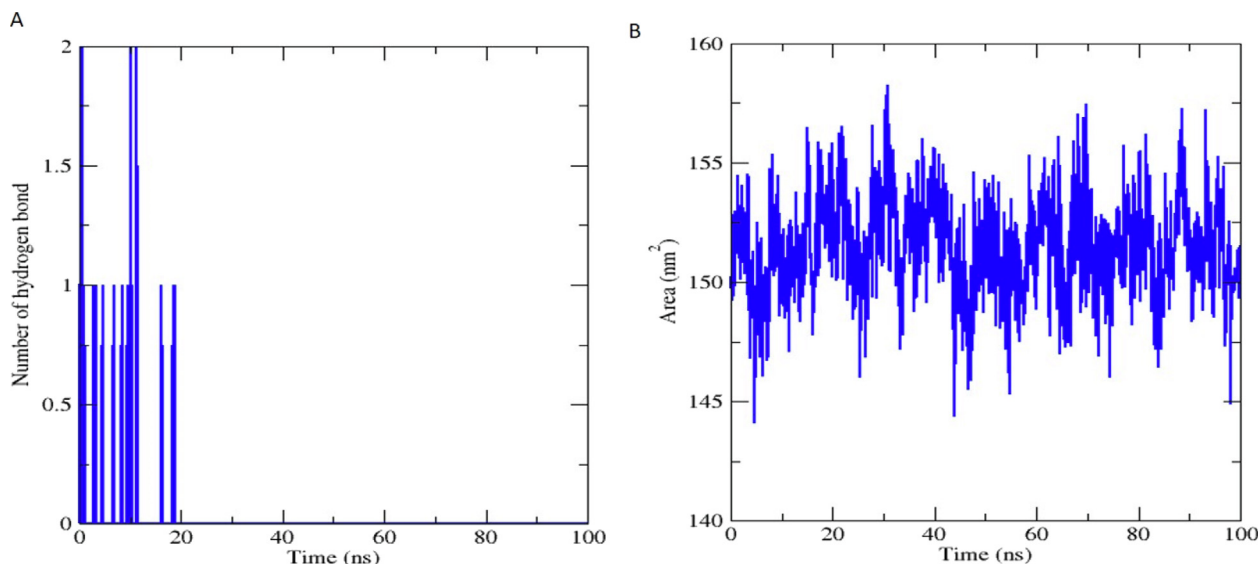


Fig. 7. Number of hydrogen bonds of the 3CLpro-inhibitor complex until 0–100 ns [A]. Y-axis is showing the calculated number of hydrogen bonds while X-axis is showing variation with respect to time in 0–100 ns (ns) during molecular dynamic simulations. Solvent accessible surface area (SASA) of 3CLpro protein [B]. Y-axis is showing the thermodynamic calculations of changes in 3CLpro surface area in nanometers square (nm^2) (Å) while X-axis is showing the residues stability time during 0–100 ns simulation time span.

Table 4
Binding free energies of the 3CLpro protein and Forsythoside A complex.

GB				PB			
Complex				Complex			
Energy component	Average	Std.Dev.	Std.Err.of Mean	Energy component	Average	Std. Dev.	Std.Err.of Mean
VDWAALS	−2547.3127	26.4445	3.6445	VDWAALS	−2547.3127	26.4445	2.6445
EEL	−22027.5023	77.5510	7.7551	EEL	−22027.5023	77.5510	7.7551
EGB	−2492.7232	77.0380	7.7038	EPB	−2374.3593	77.3967	7.7397
ESURF	87.4529	2.4109	0.2411	ENPOLAR	67.5279	0.7833	0.0783
ΔG gas	−24574.8150	77.1664	7.7166	ΔG gas	−24574.8150	77.1664	7.7166
ΔG solv	−2406.2703	75.2741	7.5274	ΔG solv	−2306.8314	77.7533	7.6753
Δ TOTAL	−26981.0853	38.4902	3.8490	Δ TOTAL	−26881.6464	40.9350	4.0935
Receptor (3CLpro)				Receptor (3CLpro)			
Energy component	Average	Std.Dev.	Std.Err.of Mean	Energy component	Average	Std.Dev.	Std.Err.of Mean
VDWAALS	−2493.8350	26.0516	2.6052	VDWAALS	−2493.8350	26.0516	2.6052
EEL	−21737.8840	77.2383	7.7238	EEL	−21737.8840	77.2383	7.7238
EGB	−2491.4093	76.1332	7.6133	EPB	−2374.1947	76.5568	7.6557
ESURF	87.6007	2.3439	0.2344	ENPOLAR	67.7287	0.7642	0.0764
ΔG gas	−24231.7190	76.0024	7.4513	ΔG gas	−24231.7190	76.0024	7.6002
ΔG solv	−2403.8086	74.5125	7.4513	ΔG solv	2306.4661	75.9236	7.5924
Δ TOTAL	−26635.5276	38.5751	3.8575	Δ TOTAL	−26538.1851	41.0493	4.1049
Ligand (Forsythoside A)				Ligand (Forsythoside A)			
VDWAALS	−14.0428	1.4837	0.1484	VDWAALS	−14.0428	1.4837	0.1484
EEL	−212.8127	4.7534	0.4753	EEL	−212.8127	4.7534	0.4753
EGB	−83.8298	2.6245	0.2624	EPB	−84.3225	2.6360	0.2636
ESURF	5.2257	0.0985	0.0098	ENPOLAR	4.2681	0.0670	0.0067
ΔG gas	−226.8556	4.8768	0.4877	ΔG gas	−226.8556	4.8768	0.4877
ΔG solv	−78.6040	2.5775	0.2578	ΔG solv	−80.0544	2.6041	0.2604
Δ TOTAL	−305.4596	3.9692	0.3969	Δ TOTAL	−306.9100	4.0704	0.4070
Difference (Complex-Receptor-Ligand)				Difference (Complex-Receptor-Ligand)			
VDWAALS	−39.4349	3.6756	0.3676	VDWAALS	−39.4349	3.6756	0.3676
EEL	−76.8056	8.3016	0.8302	EEL	−76.8056	8.3016	0.8302
EGB	−81.5158	5.0432	0.5043	EPB	84.1580	5.2030	0.5203
ESURF	−5.3735	0.2067	0.0207	ENPOLAR	−4.4689	0.1431	0.0143
ΔG gas	−116.2404	8.3345	0.8334	EDISPER	0	0	0
ΔG solv	76.1423	4.9919	0.4992	ΔG gas	−116.2404	8.3345	0.8334
Δ TOTAL	−40.0981	4.7084	0.484	ΔG solv	79.6891	5.1452	0.5145
				Δ TOTAL	−36.5514	5.1405	0.5140

* GB = The generalized Born model, *PB = The poisson-Boltzmann model, Std.Dev = Standard deviation.

attractive force based energies and is estimated as -4.4689 kcal/mol and Zero kcal/mol. For each model, MM-based energy components for the selected bounded conformation of 3CLpro receptor and Forsythoside A are tabulated in Table 4.

4. Discussion

As it is a global pandemic, SARS-CoV-2 infections emerged as pneumonia and fever in China and now reached in other countries

and a large number of people are affected and died in the last few months, WHO has described the large figures of SARS-CoV-2 / COVID-19 patients, deaths and recoveries around the globe along with the updates of vaccinations around the world (Organization World Health, 2021). As the virus was not limited to only one country or a state so its different strains make it difficult to develop any drug or vaccine which could completely treat the SARS-CoV-2 infection (Liu et al., 2020). Possible available treatments are antiviral drugs to treat different patients and another successful treatment is plasma technique as the final option for COVID-19 patients (Liu et al., 2020). Precautionary vaccination, wearing face-masks, use of sanitisers are highly encouraged to minimize the spread of COVID-19.

The previously available drugs repurposing is the most acceptable methodologies in the current scenario when there is no specific treatment for COVID-19, several *in silico* investigations have been performed to point out the potential drug-like therapeutics (Wu et al., 2020; Zhang et al., 2020). China has prescribed the Chinese traditional medicine and found effective outcomes in the control of COVID-19 along with the strict safety measures (Yang et al., 2020). The Chinese herbs were already famous for the treatment of respiratory diseases (Wang and Liu, 2014). Table 1 shows phytochemicals extracted from most of the Chinese medicinal plants, each compound is studied previously for CoV infections and other viral diseases, so this study is conducted to understand the mechanism of drug interaction with 3CLpro of SARS-CoV-2. It's highly required to find out a potential drug which should be from the natural source because it would be safer and better tolerable with historical background to treat different illnesses and acceptable in different cultures (Mani et al., 2020).

The selected target protein (PDB ID: 6LU7) for this study is 3CLpro a novel target for SARS-CoV-2 infections, significant research has been conducted on achieving the main protease inhibitors which could be potential drugs for SARS-CoV-2 and several pharmaceutical companies has developed antiviral drugs from different sources for SARS-CoV-2 and most of them are yet in clinical trials (Liu et al., 2020; Tu et al., 2020). 3CLpro inhibitors for SARS-CoV-2 could block the entry of the virus into the host and stops their replication and translation activity (Báez-Santos et al., 2015; Ziebuhr et al., 2000). Molecular docking is performed to screen a potential 3CLpro inhibitor for SARS-CoV-2 by MOE software (Vilar et al., 2008) and resulted dock scores represent the best binding capacity of ligands in the substrate-binding active site of the target protein. Summary of docking results of 10 selected compounds is shown in Table 2 and 2D plots of protein-ligand interactions for the best-docked ligand is shown in Fig. 3.

ADMET profile of the selected top-scored 10 compounds is shown in Table 3. Each compound is evaluated with respect to drug-likeness, lipophilicity, water-solubility, pharmacokinetics, toxicity estimations along with the medicinal chemistry prospective to decrease the chance of rejection of a selected lead compound (Forsythoside A) in the drug development phase. Identified lead compound followed the maximum parameters of ADMET profile with a little violation. In this study, the selected lead compound highlighted the molecular mechanism of 3CLpro inhibition to provide the direction for the novel significant therapeutics in the prospective of SARS-CoV-2 infection. Several phytochemical studies have presented the idea that most of the natural compounds are highly acceptable but do not fulfil the criteria of drug-likeness, so it's important to check the toxicity of compounds which is acceptable in the case of selected lead compounds (Katiyar et al., 2012; M. Sharifi-Rad et al., 2020). According to the molecular docking outcomes, it is concluded that the selected lead compound "Forsythoside A" from a natural

source could be a significant 3CLpro inhibitor of SARS-CoV-2 infection (Fig. 3).

Selected lead compound by the *In silico* screening (Figs. 4–7) was subjected to MD simulations at 100 ns. Fig. 4 shows the superimposed structural analysis at 0 ns and 100 ns MD simulations of the selected lead compound bound to 3CLpro of SARS-CoV-2. It is clearly illustrating the surface of 3CLpro and conformational changes of the lead compound during MD simulations until 100 ns. To understand conformational changes of the selected complex during MD simulations at the atomic level, RMSD, RMSF, Rg, BF, HBs and SASA plots of 3CLpro bound with the selected lead compound are explained significantly and also described the superimposition of lead compound binding poses at 10 ns interval within 3CLpro cavity approving the selected pocket correlates the docked results.

RMSD measures of the 3CLpro-lead compound showed an increase for a short time span at 1.8 – 3.6 Å from the start of simulations till 0.8 ns then shows very little deviations. The system gets stabilize at average values of RMSD 2.21 Å is shown in Fig. 5 (A). RMSF plot showed fluctuation between 50 and 300 amino acid residues, most of the fluctuation were observed in the loop region in and around the binding cavity that might aid in the suitable conformational pose for binding with lead compound.

Comparative analysis of the plots generated at different ns of 3CLpro bound (3CLpro-lead compound) with unbound-state of 3CLpro revealed important structural turns and twists. By the application of CADD strategy, the following retrieved information will help the researcher to move towards the development of the selected lead compound "Forsythoside A" as a potential drug for SARS-CoV-2 infection.

5. Conclusions

Forsythoside A, a natural compound extracted from *Forsythia suspense*, is selected as a lead compound by an integrated drug design pipeline. It is a medicinal compound affiliated with multiple pharmacological activities. Molecular docking investigation estimated ADMET profile and MD simulation analysis at 0–100 ns has depicted the maximum potential of lead compound as a substantial anti-SARS-CoV-2 drug with respect to 3CLpro inhibition mechanism. Moreover, its significance with respect to the medicinal perspective of viral infections has been studied previously while this *in silico* study confirms the activity of Forsythoside A as a 3CLpro inhibitor and could be repurposed for SARS-CoV-2 infections. It is highly recommended to test Forsythoside A in the laboratory for its inhibitory activity against 3CLpro of SARS-CoV-2.

Funding

This project was funded by the Deanship of Scientific Research (DSR) at King Abdulaziz University, Jeddah, Saudi Arabia, under grant no. (GCV19-46-1441). The authors, therefore, acknowledge with thanks to DSR for technical and financial support.

Declaration of Competing Interest

The authors declare that they have no known competing financial interests or personal relationships that could have appeared to influence the work reported in this paper.

Acknowledgment

The authors would like to express their gratitude to Dr. Mazhar Sadiq and Prof. Mohammad Amjad Kamal for their assistance and support to complete this work.

References

- Ahmad, S., Ranaghan, K.E., Azam, S.S., 2019. Combating tigeicycline resistant *Acinetobacter baumannii*: A leap forward towards multi-epitope based vaccine discovery. *Eur. J. Pharm. Sci.* 132, 1–17. <https://doi.org/10.1016/j.ejps.2019.02.023>.
- Aldeghi, M., Heifetz, A., Bodkin, M.J., Knapp, S., Biggin, P.C., 2016. Accurate calculation of the absolute free energy of binding for drug molecules. *Chem. Sci.* 7 (1), 207–218.
- Anand, K., Ziebuhr, J., Wadhvani, P., Mesters, J.R., Hilgenfeld, R., 2003. Coronavirus main proteinase (3CLpro) structure: basis for design of anti-SARS drugs. *Science* (80-), 300 (5626), 1763–1767.
- Báez-Santos, Y.M., St. John, S.E., Mesecar, A.D., 2015. The SARS-coronavirus papain-like protease: Structure, function and inhibition by designed antiviral compounds. *Antiviral Res.* 115, 21–38. <https://doi.org/10.1016/j.antiviral.2014.12.015>.
- Bailly, C., 2021. Forsythosides as Essential Components of Forsythia-based Traditional Chinese Medicines Used to Treat Inflammatory Diseases and COVID-19. *World J. Tradit. Chinese Med.* 8 (1), 1.
- Bian, Y., Feng, Z., Yang, P., Xie, X.-Q., 2017. Integrated in silico fragment-based drug design: case study with allosteric modulators on metabotropic glutamate receptor 5. *AAPS J.* 19 (4), 1235–1248.
- Bibi, S., Hasan, M.M., Wang, Y.-B., Papadakos, S.P., Yu, H., 2022. Cordycepin as a Promising Inhibitor of SARS-CoV-2 RNA dependent RNA polymerase (RdRp). *Curr. Med. Chem.* 29 (1), 152–162.
- Bibi, S., Sakata, K., 2017a. An Integrated Computational Approach for Plant-Based Protein Tyrosine Phosphatase Non-Receptor Type 1 Inhibitors. *Curr. Comput. Aided. Drug Des.* 13 (4). <https://doi.org/10.2174/1573409913666170406145607>.
- Bibi, S., Sakata, K., 2017b. An Integrated Computational Approach for Plant-Based Protein Tyrosine Phosphatase Non-Receptor Type 1 Inhibitors. *Curr. Comput. Aided. Drug Des.* 13, 319–335. <https://doi.org/10.2174/1573409913666170406145607>.
- Bibi, S., Sakata, K., 2016. Current Status of Computer-Aided Drug Design for Type 2 Diabetes. *Curr. Comput. Aided-Drug Des.* 12 (2), 167–177. <https://doi.org/10.2174/1573409912666160426120709>.
- Bibi, S., Sarfraz, A., Mustafa, G., Ahmad, Z., Zeb, M.A., Wang, Y.-B., Khan, T., Khan, M. S., Kamal, M.A., Yu, H., 2020. Impact of Traditional Plants and their Secondary Metabolites in the Discovery of COVID-19 Treatment. *Curr. Pharm. Des.* 27 (9), 1123–1143. <https://doi.org/10.2174/1381612826666201118103416>.
- Biswas, P., Hasan, M.M., Dey, D., dos Santos Costa, A.C., Polash, S.A., Bibi, S., Ferdous, N., Kaium, M.A., Rahman, M.D.H., Jeet, F.K., Papadakos, S., Islam, K., Uddin, M.S., 2021. Candidate antiviral drugs for COVID-19 and their environmental implications: a comprehensive analysis. *Environ. Sci. Pollut. Res.* 28 (42), 59570–59593. <https://doi.org/10.1007/s11356-021-16096-3>.
- Bogoch, I.L., Watts, A., Thomas-Bachli, A., Huber, C., Kraemer, M.U.G., Khan, K., 2020. Pneumonia of unknown aetiology in Wuhan, China: Potential for international spread via commercial air travel. *J. Travel Med.* 27, 1–17. <https://doi.org/10.1093/jtm/taaa008>.
- Case, D.A., Babin, V., Berryman, J.T., Betz, R.M., Cai, Q., Cerutti, D.S., III, T.E., Cheatham, T.A., Darden, R.E., Duke, H., Gohlke, A.W., Goetz, S., Gusarov, N., Homeyer, P., Janowski, J., Kaus, I., Kolossvary, A., Kovalenko, T.S., Lee, S., LeGrand, T., Luchko, R., Luo, B. M., P.A.K., 2014. The FF14SB force field. *Amber* 14, 29–31.
- Chen, C.-N., Lin, C.P.C., Huang, K.-K., Chen, W.-C., Hsieh, H.-P., Liang, P.-H., Hsu, J.-A., 2005. Inhibition of SARS-CoV 3C-like protease activity by theaflavin-3,3'-digallate (TF3). Evidence-based Complement. Altern. Med. 2 (2), 209–215. <https://doi.org/10.1093/ecam/neh081>.
- Chen, Y.u., Liu, Q., Guo, D., 2020. Emerging coronaviruses: Genome structure, replication, and pathogenesis. *J. Med. Virol.* 92 (4), 418–423. <https://doi.org/10.1002/jmv.25681>.
- Cho, J.K., Curtis-Long, M.J., Lee, K.H., Kim, D.W., Ryu, H.W., Yuk, H.J., Park, K.H., 2013. Geranylated flavonoids displaying SARS-CoV papain-like protease inhibition from the fruits of *Paulownia tomentosa*. *Bioorganic Med. Chem.* 21 (11), 3051–3057. <https://doi.org/10.1016/j.bmc.2013.03.027>.
- Chou, K.-C., Wei, D.-Q., Zhong, W.-Z., 2003. Binding mechanism of coronavirus main proteinase with ligands and its implication to drug design against SARS. *Biochem. Biophys. Res. Commun.* 308 (1), 148–151. [https://doi.org/10.1016/S0006-291X\(03\)01342-1](https://doi.org/10.1016/S0006-291X(03)01342-1).
- Cortegiani, A., Ingoglia, G., Ippolito, M., Giarratano, A., Einav, S., 2020. A systematic review on the efficacy and safety of chloroquine for the treatment of COVID-19. *J. Crit. Care* 57, 279–283. <https://doi.org/10.1016/j.jcrrc.2020.03.005>.
- Corum, J., Zimmer, C., 2020. Bad News Wrapped in Protein: Inside the Coronavirus Genome A String of RNA. *N.Y. Times* 22, 1–32.
- Daina, A., Michielin, O., Zoete, V., 2017. SwissADME: A free web tool to evaluate pharmacokinetics, drug-likeness and medicinal chemistry friendliness of small molecules. *Sci. Rep.* 7, 42717. <https://doi.org/10.1038/srep42717>.
- Daina, A., Michielin, O., Zoete, V., 2014. ILOGP: A simple, robust, and efficient description of n-octanol/water partition coefficient for drug design using the GB/SA approach. *J. Chem. Inf. Model.* 54 (12), 3284–3301. <https://doi.org/10.1021/ci500467k>.
- Elmezayen, A.D., Al-Obaidi, A., Sahin, A.T., Yelekcı, K., 2020. Drug repurposing for coronavirus (COVID-19): in silico screening of known drugs against coronavirus 3CL hydrolase and protease enzymes. *J. Biomol. Struct. Dyn.* 39 (8), 2980–2992. <https://doi.org/10.1080/07391102.2020.1758791>.
- Farag, A., Wang, P., Ahmed, M., Haaham, S., 2020. Identification of FDA Approved Drugs Targeting COVID-19 Virus by Structure- Based Drug Repositioning. *JAMA - J. Am. Med. Assoc.* 323, 1061–1069. <https://doi.org/10.7551/mitpress/3215.003.0017>.
- Fatima, M., Khan, M.S., Rashid, H., Mehmood, A., Kanwal, S., Rasheed, M.A., Jamil, F., 2018. Structure Based Virtual Screening and Molecular Docking Studies for Identification of Allosteric Inhibitors against Zika Virus Protease NS2B-NS3. *Pak. J. Zool.* 50. <https://doi.org/10.17582/journal.pjz/2018.50.5.1709.1715>.
- Ferreira, J.C., Rabeh, W.M., 2020. Biochemical and biophysical characterization of the main protease, 3-chymotrypsin-like protease (3CLpro) from the novel coronavirus SARS-CoV 2. *Sci. Rep.* 10, 1–10.
- Hilgenfeld, R., 2014. From SARS to MERS: crystallographic studies on coronaviral proteases enable antiviral drug design. *FEBS J.* 281 (18), 4085–4096. <https://doi.org/10.1111/febs.12936>.
- Ho, T., Wu, S., Chen, J., Li, C., Hsiang, C., 2007. Emodin blocks the SARS coronavirus spike protein and angiotensin-converting enzyme 2 interaction. *Antiviral Res.* 74 (2), 92–101. <https://doi.org/10.1016/j.antiviral.2006.04.014>.
- Holshue, M.L., DeBolt, C., Lindquist, S., Lofy, K.H., Wiesman, J., Bruce, H., Spitters, C., Ericson, K., Wilkerson, S., Tural, A., Diaz, G., Cohn, A., Fox, LeAnne, Patel, A., Gerber, S.I., Kim, L., Tong, S., Lu, X., Lindstrom, S., Pallansch, M.A., Weldon, W.C., Biggs, H.M., Uyeki, T.M., Pillai, S.K., 2020. First case of 2019 novel coronavirus in the United States. *N. Engl. J. Med.* 382 (10), 929–936. <https://doi.org/10.1056/NEJMoa2001191>.
- Honarparvar, B., Govender, T., Maguire, G.E.M., Soliman, M.E.S., Kruger, H.G., 2014. Integrated approach to structure-based enzymatic drug design: molecular modeling, spectroscopy, and experimental bioactivity. *Chem. Rev.* 114 (1), 493–537.
- Humphrey, W., Dalke, A., Schulten, K., 1996. VMD: visual molecular dynamics. *J. Mol. Graph.* 14 (1), 33–38.
- Ismail, S., Ahmad, S., Azam, S.S., 2020. Immunoinformatics characterization of SARS-CoV-2 spike glycoprotein for prioritization of epitope based multivalent peptide vaccine. *J. Mol. Liq.* 314, 113612. <https://doi.org/10.1016/j.molliq.2020.113612>.
- Jin, Z., Du, X., Xu, Y., Deng, Y., Liu, M., Zhao, Y., Zhang, B., Li, X., Zhang, L., Duan, Y., Yu, J., Wang, L., Yang, K., Liu, F., You, T., Liu, X.X., Yang, X., Bai, F., Liu, H., Liu, X.X., Guddat, L.W., Xiao, G., Qin, C., Shi, Z., Jiang, H., Rao, Z., Yang, H., 2020a. Structure-based drug design, virtual screening and high-throughput screening rapidly identify antiviral leads targeting COVID-19. *bioRxiv* 2020.02.26.964882. <https://doi.org/10.1101/2020.02.26.964882>.
- Jin, Z., Du, X., Xu, Y., Deng, Y., Liu, M., Zhao, Y., Zhang, B., Li, X., Zhang, L., Peng, C., Duan, Y., Yu, J., Wang, L., Yang, K., Liu, F., Jiang, R., Yang, X., You, T., Liu, X., Yang, X., Bai, F., Liu, H., Liu, X., Guddat, L.W., Xu, W., Xiao, G., Qin, C., Shi, Z., Jiang, H., Rao, Z., Yang, H., 2020b. Structure of Mpro from SARS-CoV-2 and discovery of its inhibitors. *Nature* 582 (7811), 289–293. <https://doi.org/10.1038/s41586-020-2223-y>.
- Kang, K.B., Ming, G., Kim, G.J., Ha, T.K.Q., Choi, H., Oh, W.K., Sung, S.H., 2015. Jubanines F-J, cyclopeptide alkaloids from the roots of *Ziziphos jujuba*. *Phytochemistry* 119, 90–95. <https://doi.org/10.1016/j.phytochem.2015.09.001>.
- Katiyar, C., Kanjilal, S., Gupta, A., Katiyar, S., 2012. Drug discovery from plant sources: An integrated approach. *Ayu* 33 (1), 10. <https://doi.org/10.4103/0974-8520.100295>.
- Khamitov, R.A., Loginova, S.Y., Shchukina, V.N., Borisevich, S.V., Maksimov, V.A., Shuster, A.M., 2008. Antiviral activity of arbidol and its derivatives against the pathogen of severe acute respiratory syndrome in the cell cultures. *Vopr. Virusol.* 53, 9–13.
- Khan, M.S., Mehmood, B., Yousafi, Q., Bibi, S., Fazal, S., Saleem, S., Sajid, M.W., Ihsan, A., Azhar, M., Kamal, M.A., 2021. Molecular Docking studies reveals Rhein from rhubarb (*Rheum rhabarbarum*) as a putative inhibitor of ATP-binding Cassette Super Family G member 2. *Med. Chem. (Los Angeles)*, 17, 273–288. <https://doi.org/10.2174/1573406416666191219143232>.
- Kim, D., Min, J., Jang, M., Lee, J., Shin, Y., Park, C., Song, J., Kim, H., Kim, S., Jin, Y.-H., Kwon, S., 2019. Natural bis-benzylisoquinoline alkaloids-tetrandrine, fangchinoline, and cepharanthine, inhibit human coronavirus oc43 infection of mrc-5 human lung cells. *Biomolecules* 9 (11), 696. <https://doi.org/10.3390/biom9110696>.
- Kim, D.W., Seo, K.H., Curtis-Long, M.J., Oh, K.Y., Oh, J.-W., Cho, J.K., Lee, K.H., Park, K. H., 2014. Phenolic phytochemical displaying SARS-CoV papain-like protease inhibition from the seeds of *Psoralea corylifolia*. *J. Enzyme Inhib. Med. Chem.* 29 (1), 59–63. <https://doi.org/10.3109/14756366.2012.753591>.
- Kim, S., Thiessen, P.A., Bolton, E.E., Chen, J., Fu, G., Gindulyte, A., Han, L., He, J., He, S., Shoemaker, B.A., Wang, J., Yu, B.o., Zhang, J., Bryant, S.H., 2016. PubChem substance and compound databases. *Nucleic Acids Res.* 44 (D1), D1202–D1213. <https://doi.org/10.1093/nar/gkv951>.
- Kräutler, V., Van Gunsteren, W.F., Hünenberger, P.H., 2001. A fast SHAKE algorithm to solve distance constraint equations for small molecules in molecular dynamics simulations. *J. Comput. Chem.* 22, 501–508. [https://doi.org/10.1002/1096-987X\(20010415\)22:5<501::AID-JCC1021>3.0.CO;2-V](https://doi.org/10.1002/1096-987X(20010415)22:5<501::AID-JCC1021>3.0.CO;2-V).
- Law, A.H.Y., Yang, C.L.H., Lau, A.S.Y., Chan, G.C.F., 2017. Antiviral effect of forsythoside A from *Forsythia suspensa* (Thunb.) Vahl fruit against influenza A virus through reduction of viral M1 protein. *J. Ethnopharmacol.* 209, 236–247. <https://doi.org/10.1016/j.jep.2017.07.015>.
- Lee, T.-S., Allen, B.K., Giese, T.J., Guo, Z., Li, P., Lin, C., McGee, T.D., Pearlman, D.A., Radak, B.K., Tao, Y., Tsai, H.-C., Xu, H., Sherman, W., York, D.M., 2020. Alchemical binding free energy calculations in AMBER20: Advances and best practices for drug discovery. *J. Chem. Inf. Model.* 60 (11), 5595–5623. <https://doi.org/10.1021/acs.jcim.0c00613>.

- Li, H., Wu, J., Zhang, Z., Ma, Y., Liao, F., Zhang, Y., Wu, G., 2011. Forsythoside A inhibits the avian infectious bronchitis virus in cell culture. *Phyther. Res.* 25 (3), 338–342. <https://doi.org/10.1002/ptr.3260>.
- Li, S.Y., Chen, C., Zhang, H.Q., Guo, H.Y., Wang, H., Wang, L., Zhang, X., Hua, S.N., Yu, J., Xiao, P.G., Li, R.S., Tan, X., 2005. Identification of natural compounds with antiviral activities against SARS-associated coronavirus. *Antiviral Res.* 67, 18–23. <https://doi.org/10.1016/j.antiviral.2005.02.007>.
- Lin, C.-W., Tsai, F.-J., Tsai, C.-H., Lai, C.-C., Wan, L., Ho, T.-Y., Hsieh, C.-C., Chao, P.-D., 2005. Anti-SARS coronavirus 3C-like protease effects of *Isatis indigotica* root and plant-derived phenolic compounds. *Antiviral Res.* 68 (1), 36–42. <https://doi.org/10.1016/j.antiviral.2005.07.002>.
- Lipinski, C.A., Lombardo, F., Dominy, B.W., Feeney, P.J., 1997. Experimental and computational approaches to estimate solubility and permeability in drug discovery and development settings. *Adv. Drug Deliv. Rev.* 23 (1–3), 3–25.
- Liu, C., Zhou, Q., Li, Y., Garner, L.V., Watkins, S.P., Carter, L.J., Smoot, J., Gregg, A.C., Daniels, A.D., Jervey, S., Albau, D., 2020. Research and Development on Therapeutic Agents and Vaccines for COVID-19 and Related Human Coronavirus Diseases. *ACS Cent. Sci.* 6 (3), 315–331. <https://doi.org/10.1021/acscentsci.0c00272>.
- Lu, H., Stratton, C.W., Tang, Y.-W., 2020. Outbreak of pneumonia of unknown etiology in Wuhan. *J. Med. Virol.* 92 (4), 401–402. <https://doi.org/10.1002/jmv.25678>.
- Lung, J., Lin, Y.-S., Yang, Y.-H., Chou, Y.-L., Shu, L.-H., Cheng, Y.-C., Liu, H.T., Wu, C.-Y., 2020. The potential chemical structure of anti-SARS-CoV-2 RNA-dependent RNA polymerase. *J. Med. Virol.* 92 (6), 693–697. <https://doi.org/10.1002/jmv.25761>.
- Izaguirre, J.A., Catarello, D.P., Wozniak, J.M., Skeel, R.D., 2001. Langevin stabilization of molecular dynamics. *J. Chem. Phys.* 114 (5), 2090–2098. <https://doi.org/10.1063/1.1332996>.
- Mani, J.S., Johnson, J.B., Steel, J.C., Broszczak, D.A., Neilsen, P.M., Walsh, K.B., Naiker, M., 2020. Natural product-derived phytochemicals as potential agents against coronaviruses: A review. *Virus Res.* 284, 197989. <https://doi.org/10.1016/j.virusres.2020.197989>.
- March-Vila, E., Pinzi, L., Sturm, N., Tinivella, A., Engkvist, O., Chen, H., Rastelli, G., 2017. On the integration of in silico drug design methods for drug repurposing. *Front. Pharmacol.*, 298.
- Miller, B.R., McGee, T.D., Swails, J.M., Homeyer, N., Gohlke, H., Roitberg, A.E., 2012. MMPBSA.py: An efficient program for end-state free energy calculations. *J. Chem. Theory Comput.* 8 (9), 3314–3321. <https://doi.org/10.1021/ct300418h>.
- Mills, N., 2006. ChemDraw Ultra 10.0 CambridgeSoft, 100 CambridgePark Drive, Cambridge, MA 02140. www.cambridgesoft.com. Commercial Price: \$1910 for download, \$2150 for CD-ROM; Academic Price: \$710 for download, \$800 for CD-ROM. *J. Am. Chem. Soc.* <https://doi.org/10.1021/ja0697875>.
- Mody, V., Ho, J., Wills, S., Mawri, A., Lawson, L., Ebert, M.C., Fortin, G.M., Rayalam, S., Taval, S., 2021. Identification of 3-chymotrypsin like protease (3CLPro) inhibitors as potential anti-SARS-CoV-2 agents. *Commun. Biol.* 4, 1–10.
- Müller, C., Schulte, F.W., Lange-Grünweller, K., Obermann, W., Madhugiri, R., Pleschka, S., Ziebuhr, J., Hartmann, R.K., Grünweller, A., 2018. Broad-spectrum antiviral activity of the eIF4A inhibitor silvestrol against corona- and picornaviruses. *Antiviral Res.* 150, 123–129. <https://doi.org/10.1016/j.antiviral.2017.12.010>.
- Naik, V.R., Munikumar, M., Ramakrishna, U., Srujana, M., Goudar, G., Naresh, P., Kumar, B.N., Hemalatha, R., 2020. Remdesivir (GS-5734) as a therapeutic option of 2019-nCoV main protease - in silico approach. *J. Biomol. Struct. Dyn.* 39 (13), 4701–4714. <https://doi.org/10.1080/07391102.2020.1781694>.
- Ntie-Kang, F., Lifongo, L.L., Mbah, J.A., Owono, L.C.O., Megnassan, E., Mbaze, L.M., Judson, P.N., Sippl, W., Efang, S.M.N., 2013. In silico drug metabolism and pharmacokinetic profiles of natural products from medicinal plants in the Congo basin. *Silico Pharmacol.* 1, 12.
- Organization World Health, 2021. WHO Coronavirus (Covid19) [WWW Document]. World Heal. Organ. URL <https://covid19.who.int/>.
- Ou, X., Liu, Y., Lei, X., Li, P., Mi, D., Ren, L., Guo, L., Guo, R., Chen, T., Hu, J., Xiang, Z., Mu, Z., Chen, X., Chen, J., Hu, K., Jin, Q.-i., Wang, J., Qian, Z., 2020. Characterization of spike glycoprotein of SARS-CoV-2 on virus entry and its immune cross-reactivity with SARS-CoV. *Nat. Commun.* 11 (1). <https://doi.org/10.1038/s41467-020-15562-9>.
- Pang, J., Wang, M.X., Ang, I.Y.H., Tan, S.H.X., Lewis, R.F., Chen, J.-I.-P., Gutierrez, R.A., Gwee, S.X.W., Chua, P.E.Y., Yang, Q., Ng, X.Y., Yap, R.K.S., Tan, H.Y., Teo, Y.Y., Tan, C.C., Cook, A.R., Yap, J.-C.-H., Hsu, L.Y., 2020. Potential Rapid Diagnostics, Vaccine and Therapeutics for 2019 Novel Coronavirus (2019-nCoV): A Systematic Review. *J. Clin. Med.* 9, 623. <https://doi.org/10.3390/jcm9030623>.
- Park, J.-Y., Jeong, H.J., Kim, J.H., Kim, Y.M., Park, S.-J., Kim, D., Park, K.H., Lee, W.S., Ryu, Y.B., 2012a. Diarylheptanoids from *Alnus japonica* inhibit papain-like protease of severe acute respiratory syndrome coronavirus. *Biol. Pharm. Bull.* 612–00623.
- Park, J.-Y., Kim, J.H., Kim, Y.M., Jeong, H.J., Kim, D.W., Park, K.H., Kwon, H.-J., Park, S.-J., Lee, W.S., Ryu, Y.B., 2012b. Tanshinones as selective and slow-binding inhibitors for SARS-CoV cysteine proteases. *Bioorganic Med. Chem.* 20 (19), 5928–5935. <https://doi.org/10.1016/j.bmc.2012.07.038>.
- Park, J.-Y., Ko, J.-A., Kim, D.W., Kim, Y.M., Kwon, H.-J., Jeong, H.J., Kim, C.Y., Park, K.H., Lee, W.S., Ryu, Y.B., 2016. Chalones isolated from *Angelica keiskei* inhibit cysteine proteases of SARS-CoV. *J. Enzyme Inhib. Med. Chem.* 31 (1), 23–30. <https://doi.org/10.3109/14756366.2014.1003215>.
- Patel, R., Vanzara, A., Patel, N., Vasava, A., Patil, S., Rajput, K., Patel, R.S., Vanzara, A. G., Patel, N.R., Vasava, A.M., Patil, S.M., Rajput, K.S., 2020. Discovery of Fungal Metabolites Bergenin, Quercitrin and Dihydroartemisinin as Potential Inhibitors Against Main Protease of SARS-CoV-2. <https://doi.org/10.26434/chemrxiv.12523136.v1>.
- Roe, D.R., Cheatham, T.E., 2013. PTRAJ and CPPTRAJ: Software for processing and analysis of molecular dynamics trajectory data. *J. Chem. Theory Comput.* 9 (7), 3084–3095. <https://doi.org/10.1021/ct400341p>.
- Ryu, Y.B., Jeong, H.J., Kim, J.H., Kim, Y.M., Park, J.Y., Kim, D., Naguyen, T.T.H., Park, S.J., Chang, J.S., Park, K.H., Rho, M.C., Lee, W.S., 2010. Biflavonoids from *Torreya nucifera* displaying SARS-CoV 3CLpro inhibition. *Bioorganic Med. Chem.* 18, 7940–7947. <https://doi.org/10.1016/j.bmc.2010.09.035>.
- Sander, T., Frey, J., von Korff, M., Rufener, C., 2015. DataWarrior: An open-source program for chemistry aware data visualization and analysis. *J. Chem. Inf. Model.* 55 (2), 460–473. <https://doi.org/10.1021/ct500588j>.
- Sepay, N., Sepay, N., Al Hoque, A., Mondal, R., Halder, U.C., Muddassir, M., 2020. In silico fight against novel coronavirus by finding chromone derivatives as inhibitor of coronavirus main proteases enzyme. *Struct. Chem.* 31 (5), 1831–1840. <https://doi.org/10.1007/s11224-020-01537-5>.
- Sharifi-Rad, J., Rayess, Y.E., Rizk, A.A., Sadaka, C., Zgheib, R., Zam, W., Sestito, S., Rapposelli, S., Neffe-Skocińska, K., Zielińska, D., Salehi, B., Setzer, W.N., Dosoky, N.S., Taheri, Y., El Beyrouthy, M., Martorell, M., Ostrander, E.A., Suleria, H.A.R., Cho, W.C., Maroyi, A., Martins, N., 2020a. Turmeric and Its Major Compound Curcumin on Health: Bioactive Effects and Safety Profiles for Food, Pharmaceutical, Biotechnological and Medicinal Applications. *Front. Pharmacol.* 11. <https://doi.org/10.3389/fphar.2020.01021>.
- Sharifi-Rad, M., Lankatillake, C., Dias, D.A., Docea, A.O., Mahomoodally, M.F., Lobine, D., Chazot, P.L., Kurt, B., Boyunegmez Tumer, T., Catarina Moreira, A., Sharopov, F., Martorell, M., Martins, N., Cho, W.C., Calina, D., Sharifi-Rad, J., 2020b. Impact of Natural Compounds on Neurodegenerative Disorders: From Preclinical to Pharmacotherapeutics. *J. Clin. Med.* 9 (4), 1061. <https://doi.org/10.3390/jcm9041061>.
- Sharma, A.D., Kaur, I., 2020. Eucalyptol (1,8 cineole) from eucalyptus essential Oil a potential inhibitor of COVID 19 corona virus infection by molecular docking studies.
- Shen, Y.-C., Wang, L.-T., Khalil, A.T., Chiang, L.C., Cheng, P.-W., 2005. Bioactive pyranoxanthones from the roots of *Calophyllum blancoi*. *Chem. Pharm. Bull.* 53 (2), 244–247. <https://doi.org/10.1248/cpb.53.244>.
- Srinivasan, K., 2018. Cumin (*Cuminum cyminum*) and black cumin (*Nigella sativa*) seeds: Traditional uses, chemical constituents, and nutraceutical effects. *Food Qual. Saf.* 2, 1–16. <https://doi.org/10.1093/fqsafef/xyx031>.
- Suwannarach, N., Kumla, J., Sujarit, K., Pattananandecha, T., Saenjum, C., Lumyong, S., 2020. Natural bioactive compounds from fungi as potential candidates for protease inhibitors and immunomodulators to apply for coronaviruses. *Molecules* 25 (8), 1800. <https://doi.org/10.3390/molecules25081800>.
- Tokusoglu, O., 2016. Black mulberry (*Morus nigra*) phenolics and anticarcinogenicity: Anti-proliferation of black mulberry powder on selected CA lines. *J. Food Process. Technol.* 07. <https://doi.org/10.4172/2157-7110.C1.056>.
- Tsai, Y.-C., Lee, C.-L., Yen, H.-R., Chang, Y.-S., Lin, Y.-P., Huang, S.-H., Lin, C.-W., 2020. Antiviral action of tryptanthrin isolated from strobilanthes cusia leaf against human coronavirus nCoV-2019. *Biomolecules* 10 (3), 366. <https://doi.org/10.3390/biom10030366>.
- Tu, Y.F., Chien, C.S., Yarmishyn, A.A., Lin, Y.Y., Luo, Y.H., Lin, Y.T., Lai, W.Y., Yang, D. M., Chou, S.J., Yang, Y.P., Wang, M.L., Chiou, S.H., 2020. A review of sars-cov-2 and the ongoing clinical trials. *Int. J. Mol. Sci.* 21, 2657. <https://doi.org/10.3390/ijms21072657>.
- Veber, D.F., Johnson, S.R., Cheng, H.-Y., Smith, B.R., Ward, K.W., Kopple, K.D., 2002. Molecular properties that influence the oral bioavailability of drug candidates. *J. Med. Chem.* 45 (12), 2615–2623.
- Vilar, S., Cozza, G., Moro, S., 2008. Medicinal Chemistry and the Molecular Operating Environment (MOE): Application of QSAR and Molecular Docking to Drug Discovery. *Curr. Top. Med. Chem.* 8, 1555–1572. <https://doi.org/10.2174/156802608786786624>.
- Wang, J., 2020. Fast Identification of Possible Drug Treatment of Coronavirus Disease-19 (COVID-19) through Computational Drug Repurposing Study. *J. Chem. Inf. Model.* 60 (6), 3277–3286. <https://doi.org/10.1021/acs.jcim.0c00179>.
- Wang, M., Cao, R., Zhang, L., Yang, X., Liu, J., Xu, M., Shi, Z., Hu, Z., Zhong, W., Xu, X., Xiao, G., 2020. Remdesivir and chloroquine effectively inhibit the recently emerged novel coronavirus (2019-nCoV) in vitro. *Cell Res.* 30 (3), 269–271. <https://doi.org/10.1038/s41422-020-0282-0>.
- Wang, X.G., Liu, Z.J., 2014. Prevention and treatment of viral respiratory infections by traditional Chinese herbs. *Chin. Med. J. (Engl)* 127, 1344–1350. <https://doi.org/10.3760/cma.j.issn.0366-6999.2013.2029>.
- Wang, X., Li, X., Wang, X., Chen, L., Ning, E., Fan, Y., Wang, H., Chen, T., Wang, W., 2021. Experimental study of Forsythoside A on prevention and treatment of avian infectious bronchitis. *Res. Vet. Sci.* 135, 523–531. <https://doi.org/10.1016/j.rvsc.2020.11.009>.
- Wilson, G.L., Lill, M.A., 2011. Integrating structure-based and ligand-based approaches for computational drug design. *Future Med. Chem.* 3 (6), 735–750.
- Wu, C., Liu, Y., Yang, Y., Zhang, P., Zhong, W., Wang, Y., Wang, Q., Xu, Y., Li, M., Li, X., Zheng, M., Chen, L., Li, H., 2020. Analysis of therapeutic targets for SARS-CoV-2 and discovery of potential drugs by computational methods. *Acta Pharm. Sin.* B, 10 (5), 766–788.
- Yan, R., Zhang, Y., Li, Y., Xia, L., Guo, Y., Zhou, Q., 2020. Structural basis for the recognition of SARS-CoV-2 by full-length human ACE2. *Science* (80- 367) (6485), 1444–1448.

- Yang, Q.-Y., Tian, X.-Y., Fang, W.-S., 2007. Bioactive coumarins from *Boenninghausenia sessilicarpa*. *J. Asian Nat. Prod. Res.* 9 (1), 59–65. <https://doi.org/10.1080/10286020500382397>.
- Yang, Y., Islam, M.S., Wang, J., Li, Y., Chen, X., 2020. Traditional Chinese medicine in the treatment of patients infected with 2019-new coronavirus (SARS-CoV-2): A review and perspective. *Int. J. Biol. Sci.* 16 (10), 1708–1717. <https://doi.org/10.7150/ijbs.45538>.
- Yang, Z., Wu, N., Fu, Y., Yang, G., Wang, W., Zu, Y., Efferth, T., 2010. Anti-infectious bronchitis virus (ibv) activity of 1, 8-cineole: Effect on nucleocapsid (n) protein. *J. Biomol. Struct. Dyn.* 28 (3), 323–330. <https://doi.org/10.1080/07391102.2010.10507362>.
- Yao, T.-T., Qian, J.-D., Zhu, W.-Y., Wang, Y., Wang, G.-Q., 2020. A systematic review of lopinavir therapy for SARS coronavirus and MERS coronavirus—A possible reference for coronavirus disease-19 treatment option. *J. Med. Virol.* 92 (6), 556–563. <https://doi.org/10.1002/jmv.25729>.
- Yi, L., Li, Z., Yuan, K., Qu, X., Chen, J., Wang, G., Zhang, H., Luo, H., Zhu, L., Jiang, P., Chen, L., Shen, Y., Luo, M., Zuo, G., Hu, J., Duan, D., Nie, Y., Shi, X., Wang, W., Han, Y., Li, T., Liu, Y., Ding, M., Deng, H., Xu, X., 2004. Small Molecules Blocking the Entry of Severe Acute Respiratory Syndrome Coronavirus into Host Cells. *J. Virol.* 78 (20), 11334–11339.
- Yin, J., Li, G., Li, J., Yang, Q., Ren, X., 2011. In vitro and in vivo effects of *Houttuynia cordata* on infectious bronchitis virus. *Avian Pathol.* 40 (5), 491–498. <https://doi.org/10.1080/03079457.2011.605107>.
- Yousafi, Q., Batool, J., Khan, M.S., Perveen, T., Sajid, M.W., Hussain, A., Mehmood, A., Saleem, S., 2020. In Silico Evaluation of Food Derived Bioactive Peptides as Inhibitors of Angiotensin Converting Enzyme (ACE). *Int. J. Pept. Res. Ther.* 27 (1), 341–349. <https://doi.org/10.1007/s10989-020-10090-y>.
- Youssef, H., Alghamdi, N., Ezzat, M.A., El-Bary, A.A., Shawky, A.M., 2021. Study on the SEIQR model and applying the epidemiological rates of COVID-19 epidemic spread in Saudi Arabia. *Infect. Dis. Model.* 6, 678–692.
- Youssef, H.M., Alghamdi, N., Ezzat, M.A., El-Bary, A.A., Shawky, A.M., 2022. A proposed modified SEIQR epidemic model to analyze the COVID-19 spreading in Saudi Arabia. *Alexandria Eng. J.* 61 (3), 2456–2470. <https://doi.org/10.1016/j.aej.2021.06.095>.
- Youssef, H.M., Alghamdi, N.A., Ezzat, M.A., El-Bary, A.A., Shawky, A.M., 2020a. A modified SEIR model applied to the data of COVID-19 spread in Saudi Arabia. *AIP Adv.* 10, 7018–7044. <https://doi.org/10.1063/5.0029698>.
- Youssef, H.M., Alghamdi, N.A., Ezzat, M.A., El-Bary, A.A., Shawky, A.M., 2020b. A new dynamical modeling SEIR with global analysis applied to the real data of spreading COVID-19 in Saudi Arabia. *Math. Biosci. Eng.* 17, 7018–7044.
- Yu, M.-S., Lee, J., Lee, J.M., Kim, Y., Chin, Y.-W., Jee, J.-G., Keum, Y.-S., Jeong, Y.-J., 2012. Identification of myricetin and scutellarein as novel chemical inhibitors of the SARS coronavirus helicase, nsP13. *Bioorganic Med. Chem. Lett.* 22 (12), 4049–4054. <https://doi.org/10.1016/j.bmcl.2012.04.081>.
- Zhang, D.-H., Wu, K.-L., Zhang, X., Deng, S.-Q., Peng, B., 2020. In silico screening of Chinese herbal medicines with the potential to directly inhibit 2019 novel coronavirus. *J. Integr. Med.* 18 (2), 152–158. <https://doi.org/10.1016/j.joim.2020.02.005>.
- Zhou, P., Yang, X.-L., Wang, X.-G., Hu, B., Zhang, L., Zhang, W., Si, H.-R., Zhu, Y., Li, B., Huang, C.-L., Chen, H.-D., Chen, J., Luo, Y., Guo, H., Jiang, R.-D., Liu, M.-Q., Chen, Y., Shen, X.-R., Wang, X.-I., Zheng, X.-S., Zhao, K., Chen, Q.-J., Deng, F., Liu, L.-L., Yan, B., Zhan, F.-X., Wang, Y.-Y., Xiao, G.-F., Shi, Z.-L., 2020. A pneumonia outbreak associated with a new coronavirus of probable bat origin. *Nature* 579 (7798), 270–273. <https://doi.org/10.1038/s41586-020-2012-7>.
- Zhuang, M., Jiang, H., Suzuki, Y., Li, X., Xiao, P., Tanaka, T., Ling, H., Yang, B., Saitoh, H., Zhang, L., Qin, C., Sugamura, K., Hattori, T., 2009. Procyanidins and butanol extract of *Cinnamomi Cortex* inhibit SARS-CoV infection. *Antiviral Res.* 82 (1), 73–81. <https://doi.org/10.1016/j.antiviral.2009.02.001>.
- Ziebuhr, J., Snijder, E.J., Gorbalenya, A.E., 2000. Virus-encoded proteinases and proteolytic processing in the Nidovirales. *J. Gen. Virol.* <https://doi.org/10.1099/0022-1317-81-4-853>.